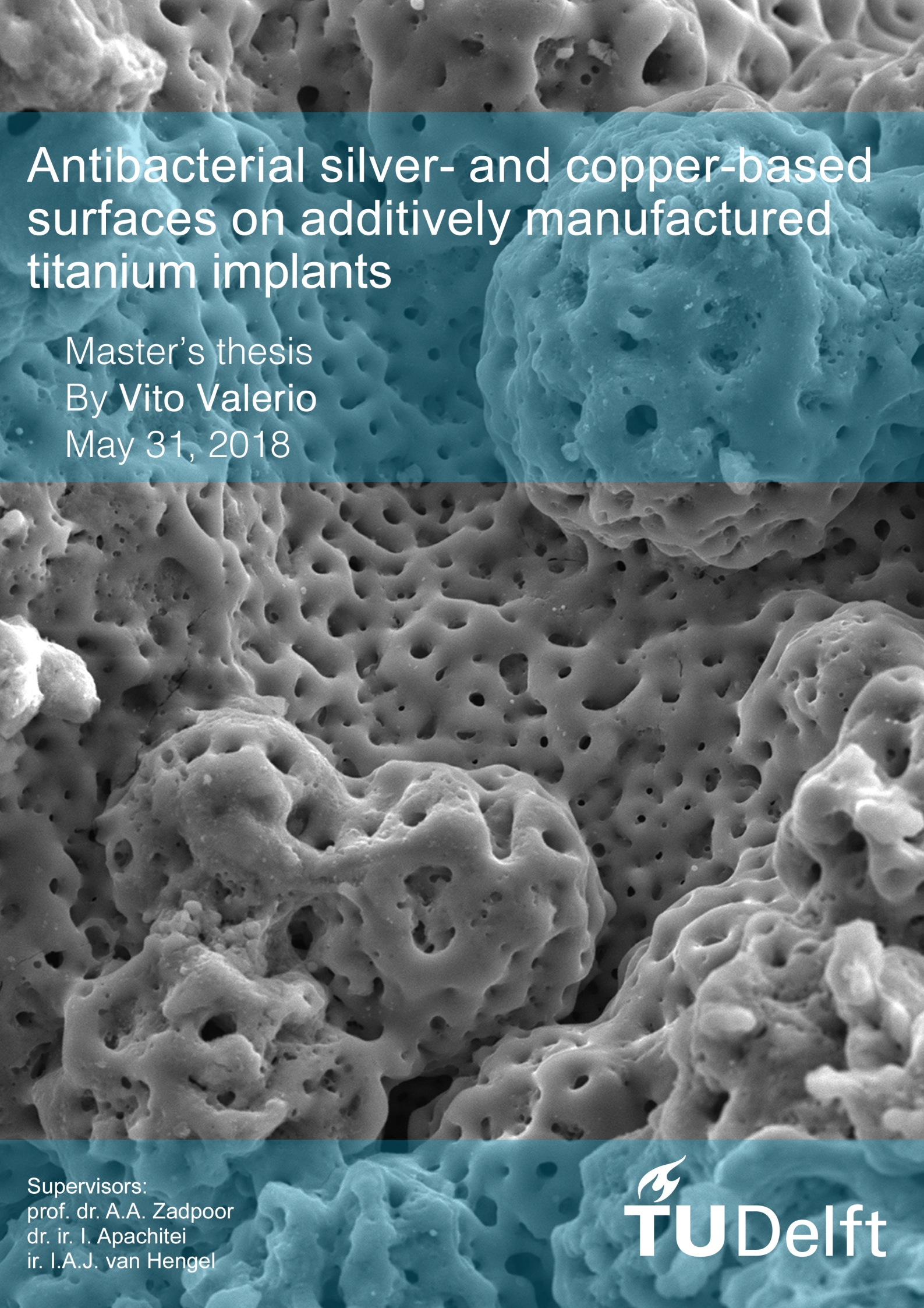

Antibacterial silver- and copper-based surfaces on additively manufactured titanium implants

Master's thesis

By Vito Valerio

May 31, 2018

Supervisors:
prof. dr. A.A. Zadpoor
dr. ir. I. Apachitei
ir. I.A.J. van Hengel

TU Delft

Antibacterial silver- and copper-based surfaces on additively manufactured titanium implants

By

Vito Valerio (4113667)

In partial fulfilment of the requirements for the degree of

Master of Science
In Biomedical Engineering

at the Delft University of Technology,
to be defended publicly on 31st of May 2018 at 15:00

Supervisors:
prof. dr. ir. A.A. Zadpoor
dr. ir. I. Apachitei
ir. I.A.J. van Hengel

Biomaterials and Tissue Biomechanics Section
Biomechanical Engineering Department
Faculty of Mechanical, Maritime and Materials Engineering
Delft University of Technology

Abstract

Background: The increase in orthopaedic implants, as a result of an ageing population, is accompanied by increasing numbers of implant associated infections (IAI). Current prevention and treatment procedures are not sufficient to prevent IAI, with a tremendous impact on patients' quality of life. Preventing IAI at the source of the infection, increases the effectiveness while simultaneously the quantity of the antibacterial agents can be reduced. By synthesising an antibacterial surface, the implant prevents bacteria from adhering to the implant surface as well as infection of the surrounding tissue. Silver and copper nanoparticles have limited reports of resistant bacteria. Combining both agents could aid in the combat against antibacterial resistance by attacking the bacteria with multiple mechanisms. Combining this novel prevention technique with additive manufactured implants, allow it to be compatible with the advancements in orthopaedic implant production. This study demonstrates the synthesis of self-defending implants by simultaneously incorporating silver and copper nanoparticles in a titanium oxide surface grown on additively manufactured Ti6Al4V implants.

Methods: Porous Ti6Al4V implants were designed and manufactured using selective laser melting (SLM). Using plasma electrolytic oxidation (PEO) a titanium oxide layer was grown on the entire implant surface. By addition of silver and copper nanoparticles along with calcium and phosphate in the PEO electrolyte, multifunctional surfaces were formed on the implants. The nanoparticles were added in silver to copper ratios of 0/100, 25/75, 50/50, 75/25, 100/0 and 100/100 to obtain several implant groups. The implant surface morphology was analysed using a scanning electron microscope (SEM). The composition of the oxide layer was analysed using energy dispersive X-ray spectroscopy (EDS), to demonstrate the incorporation of both silver and copper nanoparticles in the different silver to copper ratios. silver- and copper-ions release of the implants was measured in a biomimetic environment to characterise the *in vitro* ion release activity over one month. Subsequently, *in vitro* antibacterial experiments were performed, against *Methicillin-resistant Staphylococcus aureus*, a resistant and recurring pathogen in IAI. First, the antibacterial leaching activity was measured using a zone of inhibition assay. Secondly, the minimum inhibitory concentration (MIC) of silver-, copper-ions and the extent of synergy between the silver and copper ions was measured using a checkerboard assay. Finally, the bactericidal activity of the implants was quantified with a colony forming units (CFU) assessment.

Results: The PEO process resulted in the formation of an oxide layer with simultaneous incorporation of silver and copper nanoparticles. SEM and EDS analysis showed that the silver to copper ratio added to the electrolyte determined the nanoparticle ratio present in the oxide layer. The ion release showed silver- and copper-ions releasing over one month. The implants with both silver and copper nanoparticles showed a lower release of silver ions and a higher release of copper ions with respect to the implants with a single nanoparticle. The antibacterial leaching activity assessment showed limited leaching for the copper implants, good leaching for the silver implants and a decreasing leaching area when silver was combined with copper. The MIC of silver ions was 0.016 mM, of copper ions, 10 mM and combined 0.002 mM silver- and 5 mM copper-ions. Finally, the CFU assay showed adhering bacteria on all implants after 24h incubation and no inhibition against non-adhering bacteria.

Conclusions: The PEO process allowed for the simultaneous incorporation of silver and copper nanoparticles in the formed oxide layer, without affecting the porous geometry of the SLM manufactured implants. Combining silver and copper nanoparticles in the oxide layer promotes the cumulative Cu^{2+} and inhibits the Ag^{+} release. The Ag and Cu nanoparticles present in the implants did not prevent bacteria from adhering to the implants.

Contents

1 Introduction

Implant associated infections (IAI) form a major complication following orthopaedic surgery, resulting in patient morbidity and mortality [2, 3]. These nosocomial or hospital acquired infections [4], accounted for 8.4% of 17,180 reported hip revisions of which 18.9% occured within the first 3 months after surgery in the years 2012 and 2015 in the USA. For knee revisions, infections accounted for 9.3% of all 22,000 procedures and 44.8% of the revisions within the first 3 months after the surgery [5]. In 2012 total knee arthroplasty (TKA) and total hip replacements (THR) were the most and fourth most performed procedures in the OR in the USA [6]. Apart from the fact that TKA and THR form a substantial part of all complications in health care, these numbers are likely to increase greatly. It is estimated that by 2030 the amount of THR surgeries will increase with 174% and total knee arthroplasty surgeries with 673% relative to 2010 [7]. Therefore, it is highly important to develop and improve methods to prevent IAI.

IAI are mainly caused by the gram-positive bacteria *Staphylococcus-aureus* (34%), *Staphylococcus epidermidis* (32%) and *Pseudomonas Aeruginosa* (8%) [8, 9]. During surgery bacteria can be introduced to the implant area resulting in adherence onto the implant surface directly following or months after surgery. When bacteria are adhered to implant surfaces, most strains have the ability to form biofilms. These biofilms increase the resistance against antimicrobial agents and account for a far majority of microbial infections in the body [10]. A biofilm is formed when bacteria colonise on any interstitial surface and secrete proteins that form a protective shield against antibacterial agents. Thereafter the bacteria lower their metabolism which further decreases their susceptibility to antibacterial agents [11]. Biofilms decrease bacterial susceptibility to antibiotics 100 to 1000 times [12]. When a biofilm is formed on an implant, the surrounding tissue can easily become infected and as a result the only treatment is revision of the implant and removal of infected tissue [13-15]. Apart from the patient inconvenience, revision surgery is expensive and have many complications [16]. Therefore, prevention of biofilm formation and infections is of utter importance.

Current procedures to prevent IAI during orthopaedic surgeries are sterilisation of surgical instruments, systemic preoperative administration of antibiotics or local administration of antiseptics or antibiotics [17]. Antiseptics are used to remove transient organisms from the skin around the surgical incision area, including *Staphylococcus Epidermidis* [18]. The antiseptics most often used are iodine, alcohol and chlorhexidine gluconate [19]. When bacteria infiltrate the wound area bacterial adherence onto the implant should be prevented by either systemic or local delivery of antibacterial agents. Systemic delivery requires a very high dosage of the agent to obtain a sufficient dose at the site of infection leading to undesired side effects. On the contrary, local delivery of agents requires near minimal dose since it is administered at the source of the infection. For example with the use of antibiotic containing and secreting cement used for THRs [20] or antibiotic injection into the implant wound [21]. The last two strategies are also known as antibiotic prophylaxis, the use of antibiotics to prevent infections as opposed to treating infections with antibiotics [22]. Despite these prevention procedures, the infection numbers of total joint replacements are still substantial. A strategy for preventing biofilm formations is the synthesis of self-defending implants. By incorporating antibacterial agents in and on the surface of implants, the implant itself can prevent bacterial adhesion and biofilm formation on its surface.

Apart from biofilms, resistant bacterial strains make current antibacterial approaches ineffective. Bacteria that are resistant to antimicrobial agents account for over 2 million illnesses and over 23,000 deaths annually in the USA [23]. Resistant strains like *Methicillin-resistant Staphylococcus aureus* (MRSA) are often found nosocomial pathogens, that are resistant to most penicillin based antibiotics [24, 25]. Because of excessive use of antibiotics

and evolving resistance against the antibiotics, treatment of infections becomes more difficult [26]. The development of resistance in bacteria is a result of several bacterial modifications. Bacteria can secrete an enzyme-catalysed antimicrobial agent modification that destroys the agents, an efflux pump that removes the agents from the intercellular bacterial space and finally an alteration of the targets to which the agents bind [27]. As a result, single antibacterial agents may not kill these bacteria any longer. This has two consequences: firstly, it is harder to cure the patient infected with these bacteria. Secondly, these bacteria will procreate more compared to non-resistant bacteria due to the evolutionary effect [28, 29]. To effectively target resistant bacteria, simultaneous administration of multiple antimicrobial agents are explored in order to circumvent bacterial resistance mechanisms [27, 30]. By combining multiple antibacterial agents with different antibacterial properties, the chances for a bacterial strain to be resistant to both agents is a squared reduction compared to the strain being resistant to a single agent [31]. Moreover, there are also combinations that break the resistant mechanism of the strain, reimbursing the activity of the agent the bacteria were previously resistant against [32, 33]. This however is limited to that specific mechanism of resistance. Apart from combatting antibacterial resistance, combined agents have the potency to express synergistic antibacterial activity [34] .

Because of increasing bacterial resistance antibacterial agents with mechanisms other than that of antibiotics are under development [30, 33]. Metallic nanoparticles (NPs), that express multiple antibacterial mechanisms and target a broad spectrum of bacteria, including multi-drug resistant strains [30, 35]. Furthermore, there are limited reports of strains reporting resistance to NPs. Of these NPs, silver (Ag) has a high antibacterial activity often used in antibacterial research [36-38]. Furthermore copper (Cu) NPs have also shown antibacterial activity, while also expressing osteogenic promoting properties [39, 40]. Antibacterial activity of the combination of Ag and Cu show reduction of MIC against several bacteria [41-43] Therefore, Ag and Cu NPs are a promising combination for prevention of IAI. For this application, the combination of Ag and Cu NPs have never been studied.

Orthopaedic implants are generally manufactured from titanium alloys, such as Ti6Al4V [11]. To improve fixation of the implants, the fixation component of the implant is composed out of a scaffold structure, allowing bone ingrowth. Additive manufacturing is increasingly used to manufacture these implants, allowing tailored mechanical properties and an increased surface area of the implant. However, the porous nature of additively manufactured implants hampers the surface modification of these structures. Plasma electrolytic oxidation (PEO) which is an electrochemical method that grows the oxide layer on the titanium implant surface and very suitable to synthesise biofunctionalised porous structures [44]. Through the high voltage of this process, micro pores are formed in the oxide layer [45]. Ag and Cu NPs are incorporated in the oxide surface, by adding them to the electrolyte. Furthermore, the PEO process oxidizes the entire surface area of the implant homogeneously. The increased surface area produced by the additive manufacturing, offers more area to be covered with antibacterial agents, thereby improving the antibacterial activity of the implant [46].

The aim of this thesis is the synthesis, characterisation and antibacterial evaluation of Ag and Cu biofunctionalised self-defending Ti6Al4V implants.

2 Materials and methods

The methods and materials section provides an overview of the experiments supporting the aim of the research. The rationale behind the type of experiments is presented, as well as the rationale behind the chosen parameters for each experiment. An explanation is given on how these experiments have been performed and what parameters have been used.

The first section describes the implant design and manufacturing. In the second section the implant surface modification and antibacterial surface synthesis method is presented. The third section describes the biomaterial surface characterisation. In the final section, the antibacterial tests are presented. **Table 1** presents an overview and the study design.

Table 1: Study design. An overview of the study design used for this research, divided in sections, subsections and the applied methods.

Sections	Subsections	Methods
Implant manufacturing	Design	Matlab vector representation
	Additive manufacturing	Selective Laser Melting
Implant bio-functionalisation	Synthesis of antibacterial oxide surface	Plasma Electrolytic Oxidation
Surface characterisation	Surface morphology characterisation	Scanning Electron Microscopy
	Chemical composition	Energy dispersive X-ray spectroscopy
	Ion release	Inductively coupled plasma optical emission spectrometry
Antibacterial tests	Antibacterial leaching	Zone of Inhibition test
	Minimal inhibitory concentration	Checkerboard assay
	Biofilm prevention	Anti-biofilm test

2.1 *Implant design and manufacturing*

The implant was designed to have comparable properties as porous orthopaedic metal implants and to be manageable during *in-vitro* assays. Based on these specifications the following design requirements were defined. First of all, the implant had to be synthesised out of material used for orthopaedic implants. Secondly, the structure was to be composed of a scaffold structure, with interconnected porosity. The pore size of scaffolds for good bone ingrowth in orthopaedic implants is between 300-600µm [47]. Thirdly, the implants should be repetitive over the length of the implant, so it can be cut in smaller implants. This was convenient for antibacterial research and the ion release assay. Fourthly, the implant should be compatible with the existing PEO set up (**Appendix A**). The dimensions of the implant should not exceed 20cm in length, to fit in the electrolytic cell and in the SLM printer. Finally, the implants needed to be compatible for studies in a murine *in vivo* model.

Based on these requirements and to be able to accurately compare the findings of this research with the previously done experiments within this research group, the implant design presented by I.A.J. van Hengel et al. was used [46]. Details on the design process are presented in this article.

Implants were manufactured using selective laser melting (SLM), a powder based, layer by layer additive manufacturing technique, commonly used for creating complex porous titanium and titanium alloy structures [48]. The Matlab vector design was converted for the SLM printer using RDesigner software (Realize GmbH, Borchen Germany). The design was sliced in 50 μm layers, resulting in layers of single points indicating the laser focus points. After converting the design, the implants were synthesised using a SLM printer (SLM-125, Realizer GmbH, Borchen, Germany). The printer used a laser focus point to melt Ti6Al4V powder particles in that focus point. The laser (YLM-400-AC Ytterbium fiber laser, IPG Photonics Corporation, Oxford, USA) had a focal point diameter of 145 μm, laser power of 400 W with a wavelength of 1070±10 nm, laser current of 1200 mA and an exposure time of 300 μs.

For the SLM, spherical shaped grade-23 Ti6Al4V powder (AP&C, Boisbriand, Quebec, Canada), with a size distribution of 10-40 μm was used. The SLM process was performed in an argon environment, with 0.2% oxygen to prevent burning, oxide incorporation and smoke formation, intervening with the printing process. The base plate was preheated to 100˚C before printing the first 40 support layers. The orientation of the implants was vertical to avoid internal stresses in the implants and to increase the production batch size.

After printing, the residual powder, surrounding the implants, was removed with a vacuum cleaner. Subsequently the implants were removed from the baseplate by cutting the support structure. Finally, the implants were ultrasonically cleaned to remove excess Ti6Al4V powder particles for 5 minutes in consecutively acetone, 96% ethanol and demi water with a frequency of 50/60Hz (Sonorex super Ultrasonic bath, Bandelin, *Germany*).

2.2 *Implant surface biofunctionalisation*

2.2.1 *Plasma Electrolytic Oxidation*

For the synthesis of biofunctionalised implant surfaces, PEO was applied. PEO is a surface modification technique used to grow the existing oxide surface layer on e.g. titanium biomedical devices [49] or other valve metal objects [50, 51]. By using a high voltage for the electrochemical oxidation high local electric fields across the oxide layer cause plasma discharges. This is known as the breakdown of the titanium oxide layer. The breakdown causes formation of pits or micropores in the titanium oxide layer [52, 53].

The PEO set-up used was custom made [1]. A schematic representation of the electrolytic cell is presented in **FIGURE 1:**. The power source for the electrolytic oxidation was an AC (50Hz) power supply, (ACS 1500, ET Power Systems Ltd., *UK*) and monitored using a data acquisition system (National Instruments, NI SCXI-1000, Austin USA) measuring the voltage with a sample time of 1 second. The oxidation process was performed in a double walled glass electrolytic cell containing 800 ml electrolyte, a magnetic stirrer, a stainless steel cathode and the implant acting as the anode (**FIGURE 1:**). The electrolytic cell was cooled using a thermostatic bath (Thermo Haake open-bath circulator V15, Thermo Fischer, *USA*) that circulated cooling liquid to the electrolytic cell. During PEO processing the electrolyte was stirred with 500 rpm. The stainless-steel cathode was a hollow cylinder, completely submerged in the electrolyte and surrounding the implants. A conductive clamp, connected to an AlMg rod, held the implants in place. The clamps were connected either individually or in quadruplicate. To increase the productivity rate of the implants, a holder was designed and produced capable of holding four implants during the PEO process (**Appendix B**). The clamps were isolated using insulation tape, to prevent oxidation of the clamps.

The composition of the oxide layer was regulated by the electrolyte composition, the applied current and the duration of the oxidation process [49]. The electrolyte was composed of 24 g/L calcium acetate hydrate ($C_4H_6CaO_4 \cdot xH_2O$ [54]) and 4.2 g/L calcium glycerophosphate ($C_3H_7CaO_6P$ [55]) in demi water [1, 46]. Hydroxyapatite may be formed in the titanium oxide layer if the electrolyte contains calcium and phosphate ions [45]. Hydroxyapatite, $Ca_{10}(PO_4)_6(OH)_2$ is a bioactive material used for promoting osseointegration. The Ag and Cu NPs were added to the electrolyte in the ratio's presented in **Table 2**. Depending on the experimental groups 0-3.0 g/L NPs was added to the electrolyte. The Ag NPs were 65.0-75.0% silver based colloidal crystal and small bead NPs, with sodium chloride, sodium nitrate and sodium carbonate (Sigma Aldrich, *Spain*). The Cu NPs were 99.9% pure 40-60 nm diameter spherical NPs (SkySpring Nanomaterials, *USA*). After addition of the NPs, the electrolyte was stirred and sonicated to disperse the NPs in the electrolyte.

Because of the sparking the temperature of the electrolyte increased drastically, which may influence the conductivity over time. Therefore, prior to PEO processing the temperature of the electrolyte was cooled to 3°C. During the oxidation process the power was current controlled with a current density of 20.0 A/dm^2 with respect to the implant surface area. Following the oxidation process the samples were rinsed for 1 minute using tap water, followed by demi water and finally air dried using compressed air.

Table 2: Experimental groups used in this study. The PEO treated implants are labelled according to the relative amount of Ag and Cu NPs added to the electrolyte during PEO. 100% relates to the NPs used to for the synthesis of the Cu and Ag experimental groups.

Experimental groups	Description	Electrolyte	
		Ag NPs [g/L]	Cu NPs [g/L]
NT	Non-treated implants	-	-
PT	PEO treated implants	0	0
Cu	PEO with Cu NPs	0	3.00
Cu 75	PEO with 75% of Cu NPs	0	2.25
Cu 50	PEO with 50% of Cu NPs	0	1.50
AgCu 50/50	PEO with 50% Ag and 50% Cu NPs	1.50	1.50
AgCu 75/25	PEO with 75% Ag and 25% Cu NPs	2.25	0.75
AgCu 100/100	PEO with 100% Ag and 100% Cu NPs	3.00	3.00
Ag	PEO with Ag NPs	3.00	0
Ag 75	PEO with 75% of Ag NPs	2.25	0
Ag 50	PEO with 50% of Ag NPs	1.50	0

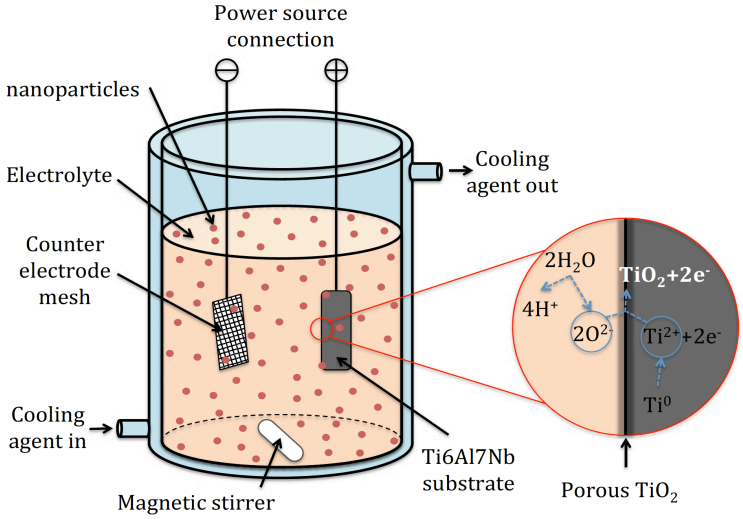

Figure 1: Schematic representation of the PEO electrolytic cell [1]. The electrolytic cell containing the electrolyte, implant, cathode and NPs. Enlarged the titanium oxidation reaction during the PEO process.

2.2.2 *Zeta potential and particle size distribution*

The zeta potential of the electrolyte is an indication for the agglomeration and the surface charge of the NPs in the electrolyte. When a charged particle is introduced to a liquid containing cations and anions, it attracts these ions based on the charge of the particle. To quantify the zeta potential, the attraction of these cations and anions is measured. A zeta potential between -30mV and 30mV, indicates agglomeration of the NPs in the electrolyte, with increasing agglomeration when approaching 0mV [56].

Both the zeta potential and particle size distribution were measured using the Zetasizer Nano (Malvern Instruments, Worcestershire, UK). A particle size range of 0.6nm-6µm could be obtained, using a 532nm laser. The Zetasizer measures the velocity of the particles by taking images of the particles in the electrolyte with a time interval of 100µs and measuring the displacement over this time interval. The particle size distribution was measured according to *Brownian motion*. The machine measures the size of the particles based on the velocity of the particles in a liquid. Small particles move fast, while large particles slow, depending on the viscosity of the liquid [56].

2.3 *Surface morphology and chemical composition*

In order to validate the quality of the titanium oxide surface and the incorporation of the NPs, the implant surfaces were characterised. First, the surface morphology of the non-treated and treated implants was characterised using scanning electron microscopy (SEM) on a JEOL JSM-IT100 (Jeol, Tokyo, Japan) microscope. The used parameters were an electron beam energy of 5-20keV, probe emission current of 50-75A and working distance of 10mm.

To determine the chemical composition, Energy-Dispersive X-ray Spectroscopy (EDS) was performed. To improve the electrical conductivity of the implants, the implants were coated with a gold layer of 5nm prior to the scanning. For each implant the chemical composition was analysed at several spots. Measurements of Ag and Cu were only taken into account when the intensity of the element succeeded 10%.

In order to distinguish between the different experimental groups and determine the ratio between Ag and Cu NPs incorporated in the implant oxide surface, an area analysis was performed. The analysis area was performed on a flat part of the surface at a magnification of 1000x. Solely the weight compositions of Ag and Cu were taken into account, in order to obtain a ratio between Ag and Cu present on the implant surface. These ratios were compared to the ratio of Ag and Cu NPs added to the electrolyte of each experimental group.

2.4 *Ion release*

To quantify the release of Ag^{+} and Cu^{2+} of the functionalised implants, an ion release measurement was performed. The release of Ag^{+} and Cu^{2+} was measured using Inductively Coupled Plasma-Optical Emission Spectrometry (ICP-OES; Spectro Arcos spectrometer, Kleve, Germany). For each group, implants of 15mm (n=3) were placed in dark Eppendorf tubes with 1 ml of Phosphate-Buffer Solution (PBS),an isotonic solution with the same ion concentration and osmotic concentration as the fluids in the human body [57]. The Eppendorf tubes were inserted in a water bath of 37°C, while kept static. After time steps of 12 hours, 1, 2, 4, 7, 14 and 28 days, each implant was transferred to a new tube containing fresh PBS, to measure the ion release between the time steps. Subsequently, the PBS samples were digested using HNO_3 to dissolve all solid matrices in the solution [58]. After the acid digestion all metals in the sample were in a dissolved state, removing potential Ag and Cu clusters in the samples. Finally, the amount of Ag and Cu ions in the samples was determined using ICP-OES.

2.5 *Antibacterial assays*

In order to evaluate the antibacterial activity of the implants several antibacterial assays were performed. First the antibacterial leaching activity was measured using a zone of inhibition (ZOI) assay. Secondly, the minimal inhibitory concentration (MIC) and synergy between Ag^{+} and Cu^{2+} was measured with a checkerboard assay. Finally, a quantitative bactericidal assay was combined with a biofilm formation assay. For all assays, the MRSA strain USA300 was used [59, 60].

2.5.1 *Sample sterilisation*

Before the antibacterial assays, the implants were cut and sterilised. First the implants were cut in samples of 7 and 15mm depending on the assay. Secondly the samples were cleaned by consecutively sonicating in 70% ethanol for 30 seconds, submersion in demiwater for 5 minutes, sonicating in demiwater for 30 seconds and air drying with compressed air. Thirdly, the samples were autoclaved for 1 hour in an oven at 110°C. Finally, the samples were stored in sterile bags until the antibacterial assays.

2.5.2 *Antibacterial leaching activity*

The antibacterial leaching activity was determined with a ZOI assay in which the antibacterial agent inhibits the growth of bacterial colonies, in growth stimulating conditions.

The assay was performed using Luria Broth growth plates. Luria Broth was heated until liquefied. Sequentially 10ml was poured onto petridishes and left to solidify. The broth was composed out of 10g/l tryptone, 5g/l yeast powder, 12g/l agar nr1 (Oxoid, thermo fischer scientific inc, UK), 10g/l sodium chloride (Fluka, Honeywell inc, New Jersey, USA) and 20 liter Super Q. For the incubation, the agar plates were covered with a swab from a Tryptic Soy Broth (TSB) solution containing approximately 5×10^{6} CFU/ml, MRSA USA300. Implants of 15mm were evenly placed in groups of 3 on the plates. After placing the implants, the plates were incubated for 24 hours at 37ºC to stimulate the growth of bacterial colony forming units (CFU).

If the bacterial colony grows, it forms an opaque layer. The area's where the bacteria cannot grow remains translucent (**Figure 2:a**). The translucent area indicates the zone of inhibition. The zone of inhibition was measured using Photoshop (Adobe Systems Incorporated, San Jose, California, USA).

2.5.3 *MIC Checkerboard assay*

The checkerboard assay is a method to assess the MIC for individual and combined antibacterial agents. Combining antibacterial agents might result in synergy, significantly lowering the MIC [34]. To control the quantity of Ag^{+} and Cu^{2+} during the assay, Ag- and Cu-nitrate ($AgNO_3$ and $Cu(NO_3)_2$) was used to measure the MIC.

The MICs were measured against MRSA USA300. The bacteria were grown in cation-adjusted Mueller Hinton (CAMH) broth until the bacteria were in log growth phase, indicated by an Optical Density at a wavelength of 600 nm (OD_{600}) of 0.08-0.100. An OD_{600} of 0.01 is equal to approximately 5×10^{6} CFU/ml. Sequentially diluted to an OD_{600} of 0.00058. Simultaneously 1mM $AgNO_3$ and 320mM $Cu(NO_3)_2$ were dissolved individually in CAMH broth. These concentrations were diluted with a ratio of 1:2 until 0.002mM $AgNO_3$ and 0.16mM $Cu(NO_3)_2$ was reached. Sequentially 50µl of CAMH broth with bacteria, 50µl of the $AgNO_3$ solution and 50µl of the $Cu(NO_3)_2$ solution were combined in a 96-wells plate, according to the rows and columns represented in **Figure 2:b**. For the positive control, 100µl clean CAMH broth was

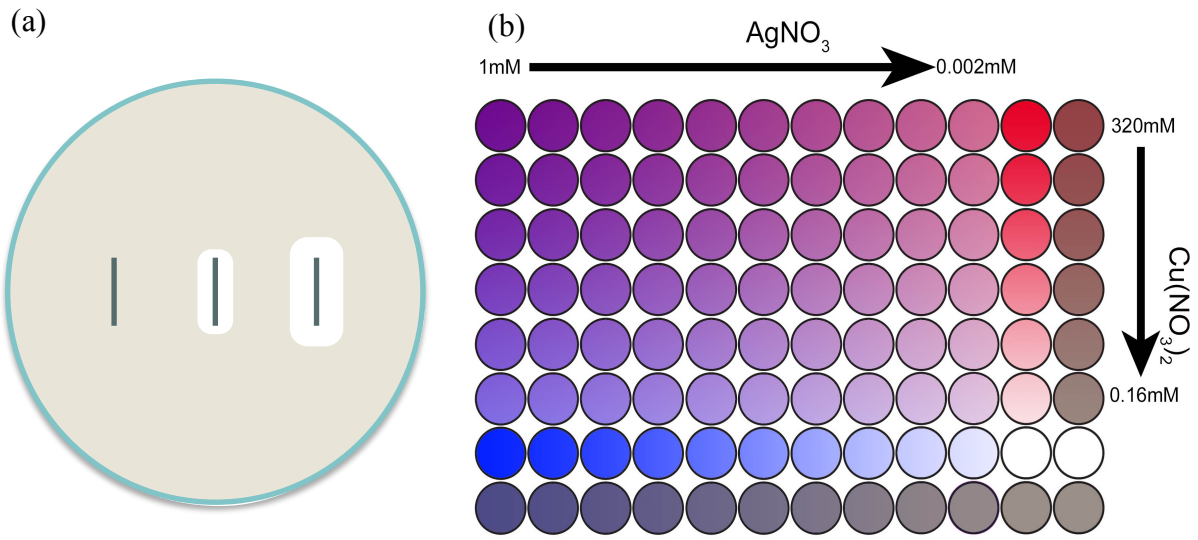

Figure 2: Schematic representations of the *in-vito* antibacterial leaching and checkerboard assessment. a) Schematic of antibacterial leaching assessment. An LB agar plate is covered with growth medium and bacterial colonies, after 24h showing from left to right no zone, a small zone and a large zone of inhibition. b) Schematic of the checkerboard assessment. A 96-well plate is filled with 150µl CAMH with approximately 1.95E4 CFU, left to right a reducing concentration of solved $AgNO_3$, from top to bottom a reducing concentration of solved $Cu(NO_3)_2$. The blue row contains exclusively $AgNO_3$ and the red column exclusively $Cu(NO_3)_2$. The darker wells contain no bacteria and the white wells no compounds. After 24h incubation the wells are measured for bacterial growth, resulting in MIC for Ag, Cu and combined Ag and Cu.

added to 50µl bacterial solution and for the negative control 150µl CAMH broth was used. Therefore, the final wells contained 150µl broth with a bacterial concentration of approximately 1.3×10^5 CFU/ml. The plates were statically incubated for 24h at 37°C.

After incubation, the wells were visually examined based on the following criteria: a large colony was scored as a 2, a small colony as 1 and a clean well as 0. Whenever a well with both Ag^+ and Cu^{2+} has a MIC that is lower than the additive concentration of the individual agents, a synergistic effect is present.

2.5.4 *Prevention of bacterial adhesion and biofilm formation*

The bactericidal- and bacteriostatic-activity and capability to prevent biofilm formation of the biofunctionalised implants were addressed in one experiment. In order to demonstrate the prevention of adhering bacteria on the biofunctionalised implants, the bacteria should adhere to the NT and PT implants. Therefore, first the bacterial inoculum concentrations where defined that showed bacteria adhering to the NT and PT implant surfaces. The lowest concentration that showed adhering bacteria would have the largest possibility to be inhibited by the biofunctionalised implants. Therefore, the biofunctionalised implants were evaluated for their ability to prevent bacteria adhering to the implant surface and inhibiting non-adherent bacteria in the inoculum using the inoculum with the lowest concentration that showed adhering bacteria on the NT and PT implants.

A fresh MRSA USA300 bacterial culture was introduced to 3 ml TSB and incubated at 37 °C to grow until it reached its log growth phase at an OD_{600} of 0.5-0.6. The TSB, containing bacteria, was combined with 1% glucose and diluted by adding TSB until the solutions reached an OD_{600} of 0.01, 0.001 and 0.0001 equivalent to approximately 5.0×10^6, 5.8×10^5 and 6.5×10^4

CFU/ml. Implants of 7 mm (n=4 per group), were submerged in 600 µl inoculum with the different concentrations and incubated for 24 hours, at 37℃ , while kept in motion.

After incubation the number of adherent and non-adherent e.g. planktonic bacteria were determined. For the analysis of adherent bacteria, the implants were cleaned three times with PBS to preserve only the adhering bacteria on the implant surfaces. These implants were then submerged in 2 ml PBS and sonicated for 1 minute at 35 kHz (*Bandelin BactoSonic 14.2, Berlin Germany*), to remove the adherent bacteria from the implants and obtain solutions containing only the adherent bacteria. To determine the CFU of non-adhering bacteria, samples were taken from the incubation inoculum. For each group an extra implant was used to characterise the biofilm formation on the implants using SEM.

Subsequently, 20 µl was taken and serial dilutions (i.e. 10^{-1} to 10^{-7}) and pipetted in lines on a blood agar growth plate. The plates were then incubated for 24 hours at 37°C. After the incubation, colonies were formed on the agar plate. Based on the amount of CFU on the plates and the dilution, the CFU/ml was calculated for each experimental group, indicating the adhesion of bacteria on the implant surfaces and the bacteriostatic and bactericidal activity in the surrounding inoculum.

The described procedure for defining the required concentration was identical to the actual assessment of the biofunctionalised implants, apart from using the different concentrations.

2.6 *Statistical analysis*

For the statistical analysis, the graphical representations and data processing, Matlab 2018b (MathWorks, Massachusetts, USA) and GraphPad Prism (GraphPad Software, La Jolla, California, USA) were used. The results were presented in mean ± standard deviation. The number of samples for each experiment is presented in the results. A one-way ANOVA test was performed for comparing different experimental groups at one time step and a two-way ANOVA for two or more time steps, using GraphPad Prism.

3 Results

3.1 *Implant*

3.1.1 *Design and manufacturing of the implant*

Based on the design requirements, the design represented in **Figure 3a** was used. This design was obtained from a previous research with a similar research set up and goal [46]. More details on the design process are presented in the publication.

The design, presented in **Figure 3a**, is vector based. The design makes use of a repetitive unit cell, repeated in the z-direction. The implant is 0.5 mm in diameter and 40 mm in length. The strut thickness was not defined in the design since it is vector based, therefore the strut thickness will result from the minimum melt pool size of the SLM printer.

The final implants differed from the 3D design, due to inaccuracies in the SLM printing process. Firstly, the surface of the implant was covered with partially melted Ti6Al4V powder particles (**Figure 3b-d**). These Ti6Al4V powder particles are not in the laser spot but are pulled into the melt pool during SLM. This resulted in the Ti6Al4V powder particles being partly incorporated in the implant surface. These partly melted Ti6Al4V powder particles formed a rougher surface and an increase in surface area compared to the 3D design. Secondly, the strut thickness varied over the print direction (length of the implant). Each layer of powder particles was melted in a flattened spherical melt pool by the laser spot with a thickness of 50 μm. This resulted in the struts to be composed of spherical parts, melted together at the narrower circumference (**Figure 3b**). The final strut thickness was 177±25 μm and diameter of the implants 668±8 μm. The final pore size of the printed implants was 379±50 μm over the major axis and 221±25 μm over the minor axis.

The post treatment consisted of sequential sonication steps in acetone, ethanol and demi water for 5 min. Based on the SEM images in **Figure 3b-d,** it was observed that the Ti6Al4V powder particles that where not melted during SLM, were removed from the implant surface.

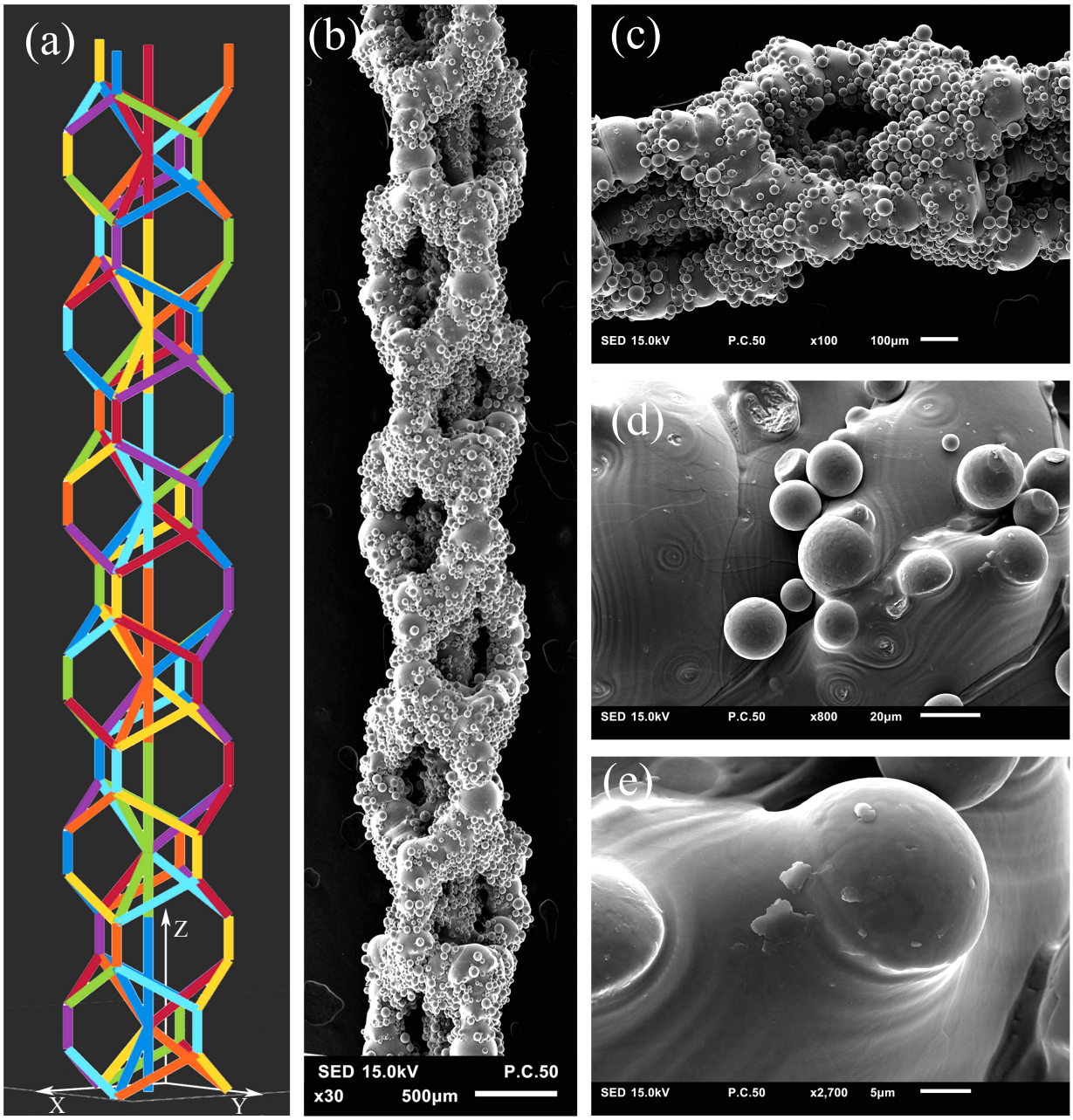

Figure 3: Design representation and SEM images of the SLM printed implants. a) The implant design is represented in vector lines. The representation is composed out of six unit cells of 1mm^3, stacked in Z-direction. b) SEM image of the implant. c) surface morphology of the implant after SLM printing and Ti6Al4V powder removal. d,e) partly melted Ti6Al4V powder particles on the implant surface.

3.1.2 *Synthesis of antibacterial surfaces*

The synthesis of the antibacterial surface was performed with PEO. The composition of the oxide layer was controlled by the voltage response and the electrolyte. For the PEO process the current density was set at 20 A/dm^2. Due to the growing oxide layer, the resistance of the implants increased. This resulted in an increase in voltage. The voltage response was measured during the process with a sample time of 1 second. The resulting averaged curve is presented in **Figure 4**.

The voltage response was characterised by four distinctive sections: the initial rapid increase in voltage, the dielectric breakdown of the oxide layer, the reduced increase in voltage and the final voltage. The obtained variables, presented in **Table 3**, were measured for each group The initial rapid increase started directly after the initial load applied to the set-up, until it reached the tipping point. It was defined to be between 1 and 6 seconds after the initial load. The initial increase had a gradient of 16.5±0.6 V/s. The tipping point corresponded to the dielectric breakdown, defined by the largest change in gradient between 5 and 10 seconds after the initial load. The breakdown voltage was at 120±4V. The reduced increase in voltage section started 100 seconds after the initial load and continued until the load was removed after 300 seconds. The gradient of this section was 0.22±0.02V/s. The final voltage was 246±6.6V, defined as the highest voltage response. The final voltages of each group with NPs were significantly lower compared to the PT voltage ($p<0.0005$). The temperature of the electrolyte was measured before and after the process. Before the process the average temperature was 5±1ºC, after the process it was increased to 9±1ºC.

To increase the production rate a new holder was created that allowed for the synthesis of up to four implants at the same instance. The schematics for this multi-holder and the final product is presented in **Appendix B**.

Table 3: The PEO process variables for each experimental group. The PEO voltage response curve is characterised by four sections.

Experimental groups	Process variables			
	Gradient 1 [V/s]	Dielectric breakdown [V]	Gradient 2 [V/s]	Final voltage [V]
PT	15.9±0.5	127±2.1	0.2±0.4	258±2.9
Cu	16.9±2.7	123±2.9	0.2±0.3	249±2.2
AgCu 25/75	17.2±3.4	119±3.0	0.2±0.3	247±4.4
AgCu 50/50	16.8±1.3	116±2.4	0.2±0.3	240±1.7
AgCu 75/25	15.7±0.9	117±3.9	0.2±0.2	241±2.8
Ag	16.5±1.5	122±3.9	0.2±0.3	245±3.2

Agglomeration of the NPs in the electrolyte was evaluated by the zeta potential and size distribution of the NPs in the electrolyte. The measurements were performed with a 10-fold diluted electrolyte. The zeta potential of both individual and combined NPs were slightly negative in the electrolyte dilution (**Figure 5**). The zeta potential of Cu NPs was -6.8±0.4mV, while that of Ag NPs was -16.8±1.0mV. The zeta potential for the combined NPs was largest for AgCu 75/25 (-16.7±0.7mV), followed by AgCu 25/75 (-14.2±0.5 mV) and finally AgCu 50/50 (-11.8±0.5mV). All groups were significantly different, except for Ag with AgCu 75/25. All values were within the -30 and 30mV range, indicating some form of agglomeration.

The size distribution, presented in **Figure 5b,** shows the mean particle size for the NPs in the electrolyte. The mean size for the Ag NPs was 4.081±0.256μm and for the Cu NPs 1.679±0.093μm in the electrolyte. The size of the Ag NPs was significantly larger compared to the other groups. The combined NPs were similar to Cu.

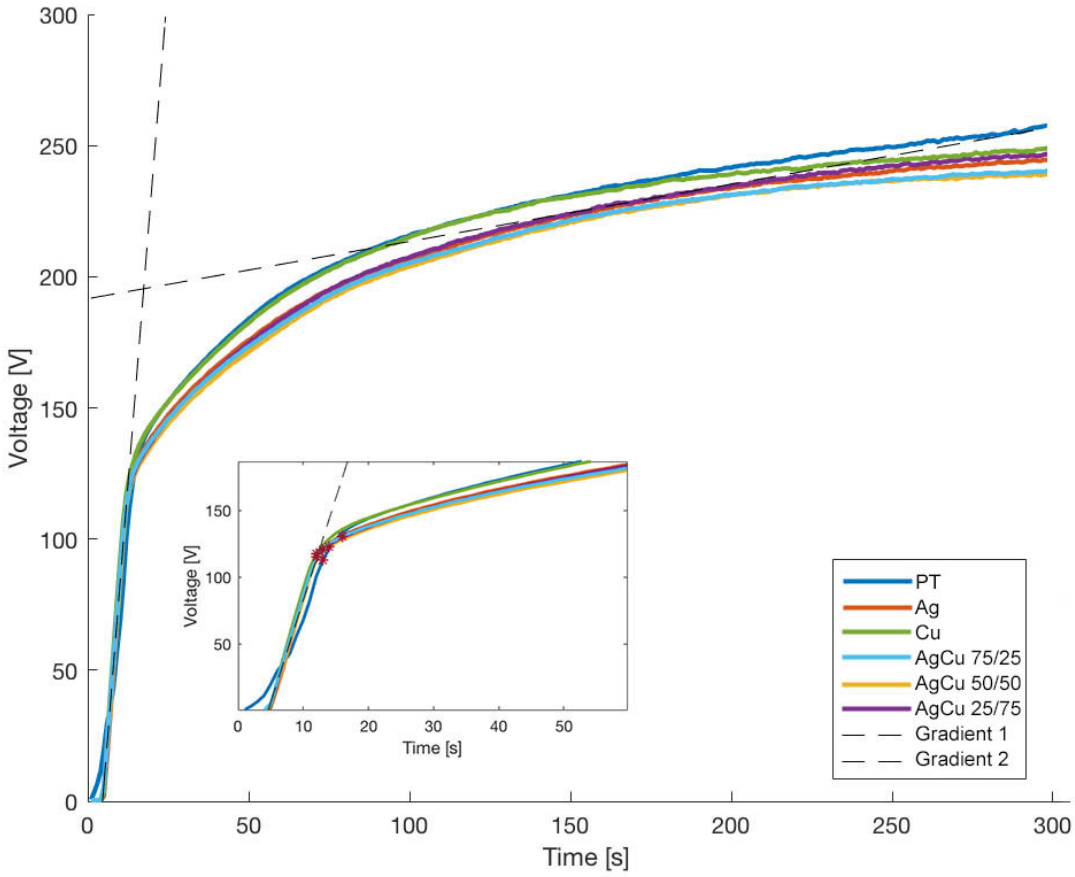

Figure 4: PEO voltage response. The average voltage response during the PEO process for all experimental groups. Enlarged is the dielectric breakdown for each group indicated with asterixes. Gradient 1 indicates the average gradient during the initial rapid increase in voltage and gradient 2 is the average of the reduced increase in voltage

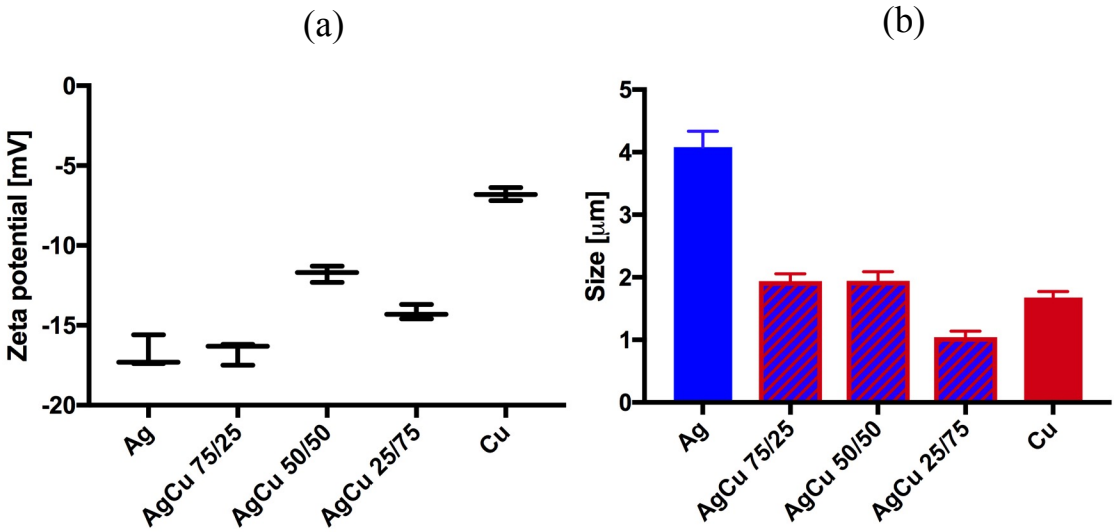

Figure 5: The zeta potential and NP size distribution in the electrolyte. a) The zeta potential measurements (n=3) of the electrolyte for the different experimental groups. b) size distribution measurements (n=3) of the NPs in the electrolyte. The electrolyte was diluted 10 times in order to obtain an accurate measurement.

3.2 *Surface characterisation*

3.2.1 *Surface morphology and chemical composition*

In **Figure 6:** the surface morphology of the PT implants is presented. The PEO treatment changed the reflective silver metallic surface of the SLM printed implants to a darker matt color. Between the different PEO treated experimental groups no difference was observed at macro scale. The implants were homogeneously covered by the TiO_2 layer (**Figure 6:a-b**). The PEO treated samples showed a micro porous and irregular surface (**Figure 6:c-d**). The partly melted Ti6Al4V powder particles were still observable and the macro pores were still present after the PEO process. The oxide layer contained a homogeneous distribution of the micropores. These micropores were caused by the dielectric breakdown of the oxide layer during the PEO process.

The chemical composition of the implant surfaces iss presented in **Figure 7**. Spot analysis was used to distinguish between the TiO_2 layer, Ag and Cu NPs incorporated in the TiO_2 layer. The results were presented in the spectrum obtained from the EDS analysis, indicating the compositions of the different spots indicated in the images. The spot analysis of the NPs showed Ag or Cu. No direct contact between Ag and Cu NPs was found for the implants with both NPs.

In order to obtain the ratio between Ag and CU NPs, an EDS area analysis was performed (**Figure 8**; n=10). The analysis included solely Ag and Cu, therefore it represents the weight ratio of Ag and Cu on the implant surface. The results are represented as weight percentage Ag and Cu measured on the implant surface, with the sum of the Ag and Cu concentration being 100%. The results showed a trend that was comparable to the Ag to Cu ratio in the electrolytes, however it did not correspond to the exact ratio's. All groups were significantly different from each other.

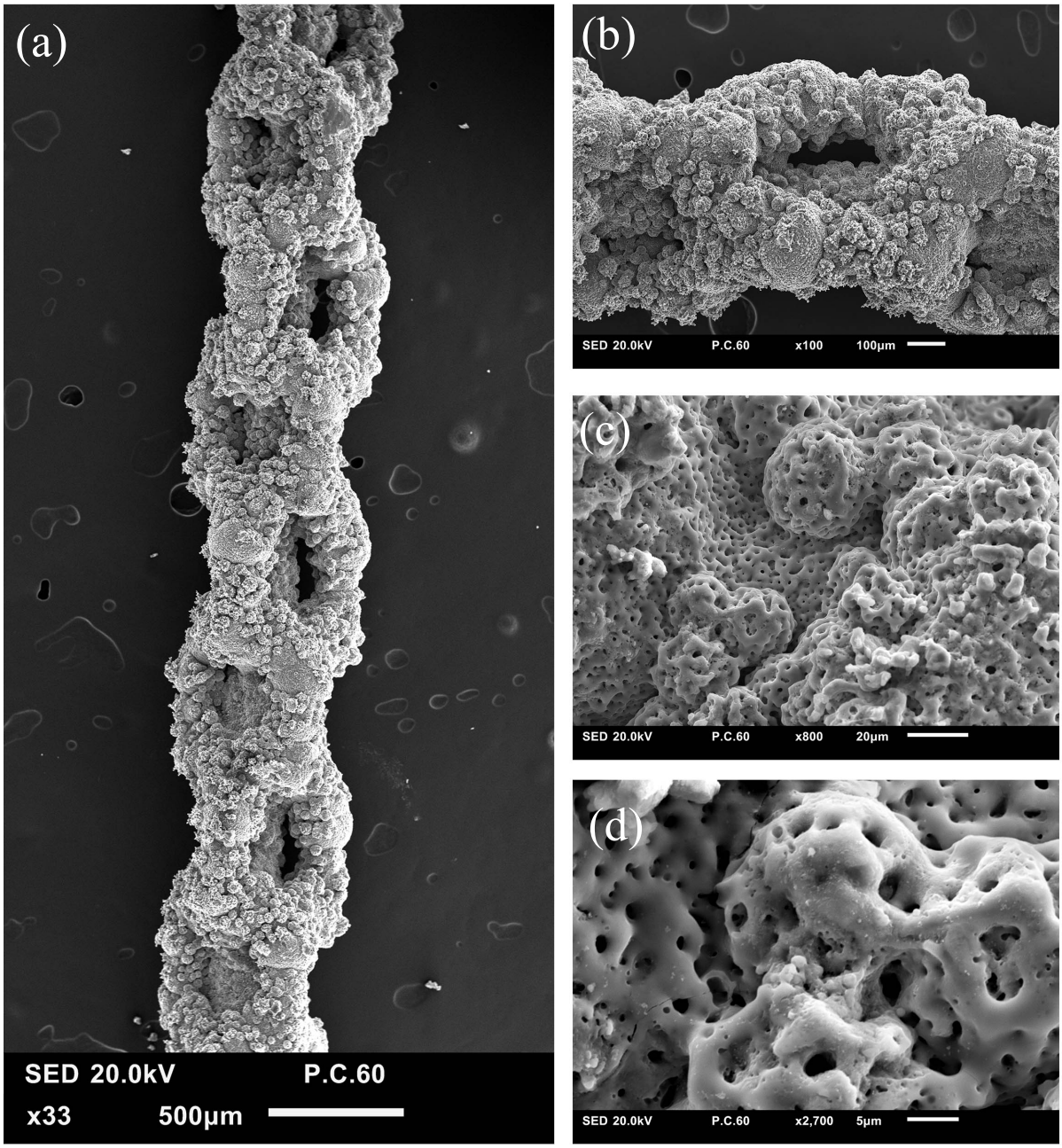

Figure 6: SEM images of PEO treated implant surface. a) SEM image of the implant. b) SEM image showing the oxidation of the entire surface including partly melted Ti6Al4V particles. c) the implant with typical PEO morphology. d) the micropores caused by the dielectric breakdown of the titanium oxide layer during PEO.

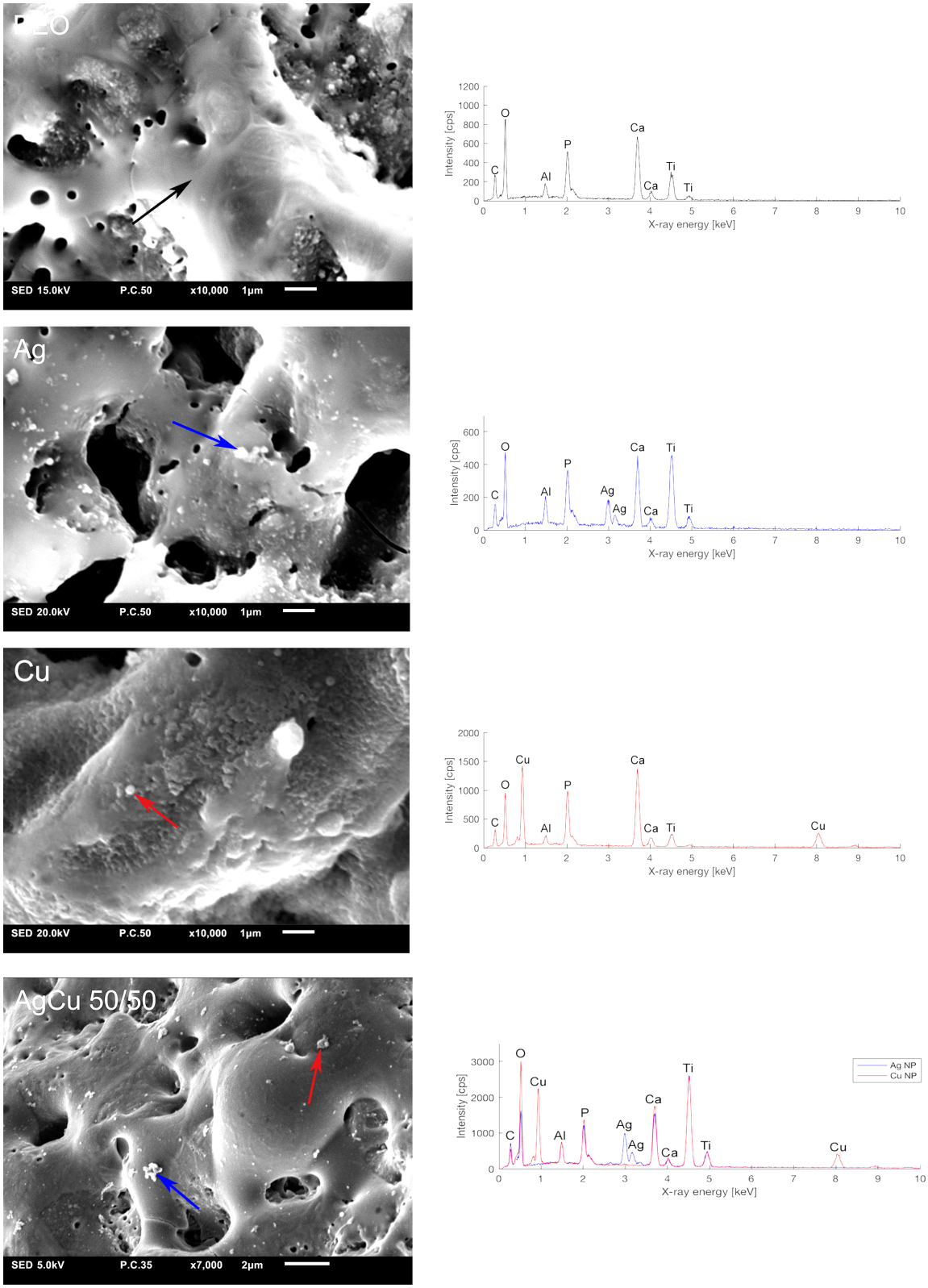

Figure 7: Chemical composition of implant surface determined by EDS. Arrows indicate the spot for EDS spot analysis. The black arrow indicates the oxide layer composition, blue the Ag NPs and red the Cu NPs.

3.2.2 *Ion release*

The release of Ag and Cu ions from 7mm long implants was measured for 12 hours, 1 day, 2-, 4-, 7-, 14- and 28-days. The Ag and Cu ions for each group are represented in **Figure 9a-b,** present the ion release after the first 12 hours for each experimental group. For the AgCu implants, the ion release showed a trend corresponding to the quantity of NPs in the electrolyte. The Ag^+ release of the Ag 50 was approximately 48% and the Ag 75 release 64% of the Ag implant. For the Cu implants, the trend was similar, with Cu 50 being 55% and Cu 75 the Cu^{2+} release was 65% of the Cu implant.

When comparing the ion release of the AgCu implants to the Ag and Cu implants with the same amount of Ag or Cu NPs, the Ag^+ release is decreased while the Cu^{2+} release is increased when combining Ag and Cu. The Ag^+ release of AgCu 75/25 was 50% of that of Ag 75 (231±30ppb and 461±95ppb; p=0.015). For AgCu 50/50 it was 56% of Ag 50 (345±66ppb and 194±56ppb; p=0.197). The Cu^{2+} release of the AgCu 25/75 implants was 211% higher compared to the Cu 75 implants (806±296ppb and 381±28ppb; p=0.051) and that of AgCu 50/50 implants was 175% higher compared to the Cu 50 implants (561±198ppb and 320±61ppb; p=0.446). This shows that for the AgCu implants the Ag^+ release is approximately halved and the Cu^{2+} is approximately doubled when compared to the solely Ag and Cu implants.

The AgCu implants show decreasing Ag^+ and Cu^{2+} release with respectively decreasing Ag and Cu on the implant surface. The Ag^+ release of the AgCu 50/50 is 84% of the AgCu 75/25 (p=0.985) and that of AgCu 25/75 is 74% of the AgCu 75/25 implant (p=0.895). The Cu^{2+} release of the AgCu 50/50 is 70% of the AgCu 25/75 implant (p=0.430) and AgCu 75/25 is 45% of the AgCu 25/75 implant (p=0.038).

Cu^{2+} and Ag^+ were released at least up to 28 days after the test was initiated (**Figure 9c-d)**. The Cu^{2+} release was higher compared to Ag^+ and showed a decrease in release approaching the 28 days. The Ag containing implants also showed Ag^+ release after 28 days.

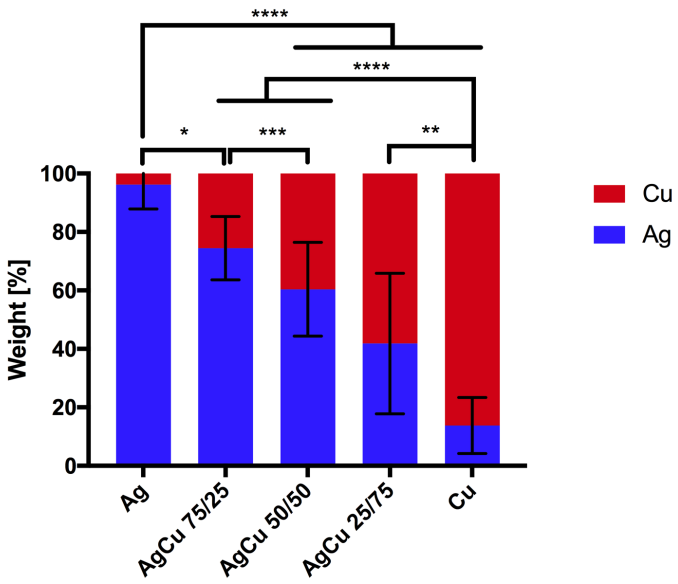

Figure 8: Quantification of AgCu ratios in implant TiO_2 layer. EDS analysis was performed solely on Ag and Cu elements (n=10).

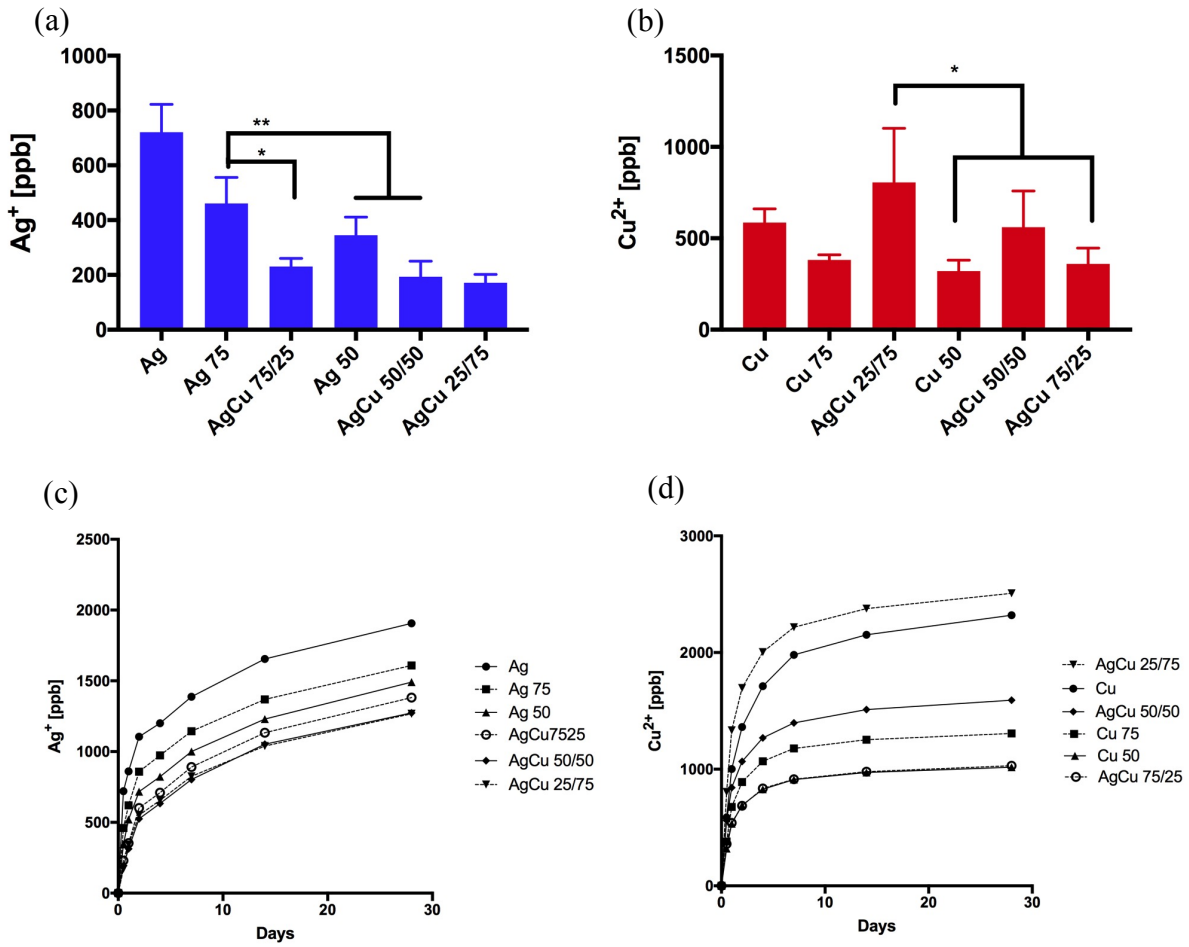

Figure 9: Ag and Cu ion release from biofunctionalised implants up to 28 days. The ion release measurements in 1ml PBS for implants of 15mm, n=3. a,b) the ion release after 12 hours for each experimental group. Blue indicates the Ag^{+} release and red the Cu^{2+} release. c) shows the cumulative Ag^{2+} release for all the copper containing implants for 28 days. d) shows the cumulative Cu^{+} release for all silver containing implants for 28 days.

3.3 *Antibacterial assays*

3.3.1 *Antibacterial leaching activity*

The leaching activity of 1.5cm long implants was measured using the zone of inhibition assay. After 24h incubation on a LB growth plates, the growing CFU formed an opaque layer, while the inhibited area remained translucent (**Figure 18**). The measured ZOI are presented in **Figure 10a**, with n=3 except for Ag 75 and Ag 50 with n=2.

The Ag containing groups showed a clear ZOI surrounding the implants that was described by an elliptical shape. The implants with solely Ag showed large ZOI. The Ag 75 ZOI was 91% of the Ag implant (1.05±0.12cm^2 and 1.12±0.10cm^2; p= 0.9998) and the Ag 50 was 91% of the Ag implant (1.01±0.00cm^2; p= 0.997). Due to small number of samples, the p-values is high. Cu implants showed a small ZOI that was just 14% of the Ag ZOI (0.16±0.24cm^2; p=0.0002).

The AgCu implants did not show a clear trend. The AgCu 75/25 showed the smallest ZOI of AgCu implants, with 54% of the Ag (0.60±0.06cm^2; p=0.046). The second smallest ZOI of the AgCu was AgCu 25/75 with 61% of the Ag (0.69±0.21cm^2; p=0.122). Thirdly the AgCu 50/50 showed a ZOI of 88% of the Ag (0.98±0.15cm^2; p=0.976) and finally the largest was the AgCu 100/100 with 140% of the Ag (1.56±0.26cm^2; p=0.104). The NT and PT implants did not have a ZOI and are therefore not presented. For this assay the AgCu 100/100 implant (**Table 2**) was added that showed the largest ZOI.

3.3.2 *MIC checkerboard assay*

The checkerboard assay was used to define the MIC of Ag^+ and Cu^{2+} against MRSA USA300. The wells contained 150µl CAMH broth with a bacterial concentration of 1.3×10^5 CFU/ml and concentration of either $AgNO_3$, $Cu(NO_3)_2$ or both, presented in **Appendix E**.

The obtained MIC for Ag^+ was 0.016mM and for Cu^{2+} it was 10mM, which is a factor 625 higher compared to Ag^+. For the combined agents the MIC were 0.002mM Ag^+ and 5mM Cu^{2+}. This is a reduction of 12.5% of the MIC for Ag^+ and 25% of MIC for Cu^{2+} to inhibit bacterial growth. The reduction in the MIC values when Ag^+ and Cu^{2+} where combined surpassed the additive effect of the individual agents. Therefore, Ag^+ and Cu^{2+} show synergistic antibacterial effects when combined.

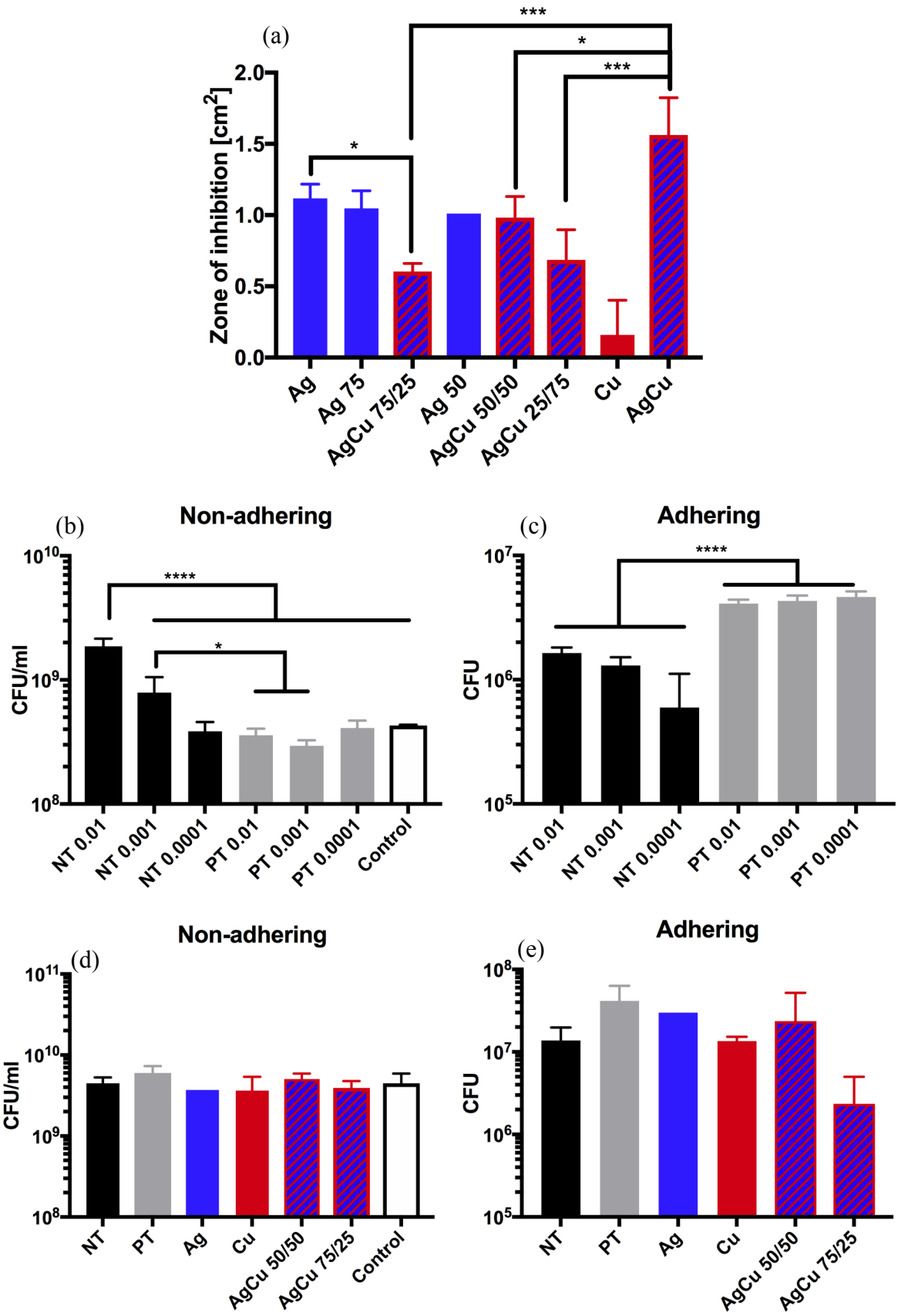

Figure 10: Leaching activity and biofilm prevention assays with log scale. All results are after 24 h incubation. a) zone of inhibition results from leaching assay for the 15mm implants. CFU count of b) non-adhering and c) adhering bacteria with different bacterial inocula. CFU count of d) non-adhering and e) adhering bacteria with an bacterial inoculum of OD0.001. n=3 per group, except for Ag 75 and Ag 50 in zone of inhibition (n=2).

3.3.3 *Prevention of bacterial adhesion and biofilm formation*

In order to assess the prevention of biofilm formation on the biofunctionalised implants, a quantitative bactericidal assay was performed. First, the minimal concentration of bacteria was defined, that showed adhering bacteria on both NT and PT implants. The CFU counts are presented in **Figure 10b-c**.

The CFU count from the incubation medium showed significantly more bacteria in the NT OD_{600} 0.01 compared to all other groups ($p<0.0001$) and NT OD_{600} 0.001 significantly higher compared to PT OD_{600} 0.001 ($p=0.0297$). The PT implants showed significantly more adhering bacteria compared to the NT implants ($p<0.0001$). The different bacterial concentration had no significant effect on the adhering bacteria for NT or PT implants.

For SEM imaging, an additional implant was incubated for each group. The adhering bacteria were fixated on the implant after the assay and SEM images are presented in **Figure 11:**. For the NT implants, the bacteria adhered most often in the transition grooves between partly melted Ti6Al4V powder particles and the implant. The most outer surfaces contained no adhering bacteria. On the PT implants the bacteria were located in larger micro pores, similar to the grooves formed by the partly melted Ti6Al4V powder particles.

Based on this experiment the bactericidal activity of Ag, Cu, AgCu 50/50 and AgCu 75/25 implants was tested f with a bacterial concentration of OD_{600} 0.0001 ($n=3$). The CFU counts for the bacteria in the medium and the adhering bacteria are presented in **Figure 10d-e**. Two of the Ag implant wells were contaminated; hence no standard deviation was given.

The CFU count for the incubation medium showed no significant difference between any of the groups. This indicated no antibacterial activity for the biofunctionalised implants. The CFU count for the adhering bacteria likewise showed no significant difference between the groups. However, the SEM images presented in **Figure 12:** showed many adhering bacteria for all implants, apart from the Ag implant. The Ag implant showed almost no adhering bacteria, based on the SEM characterisation.

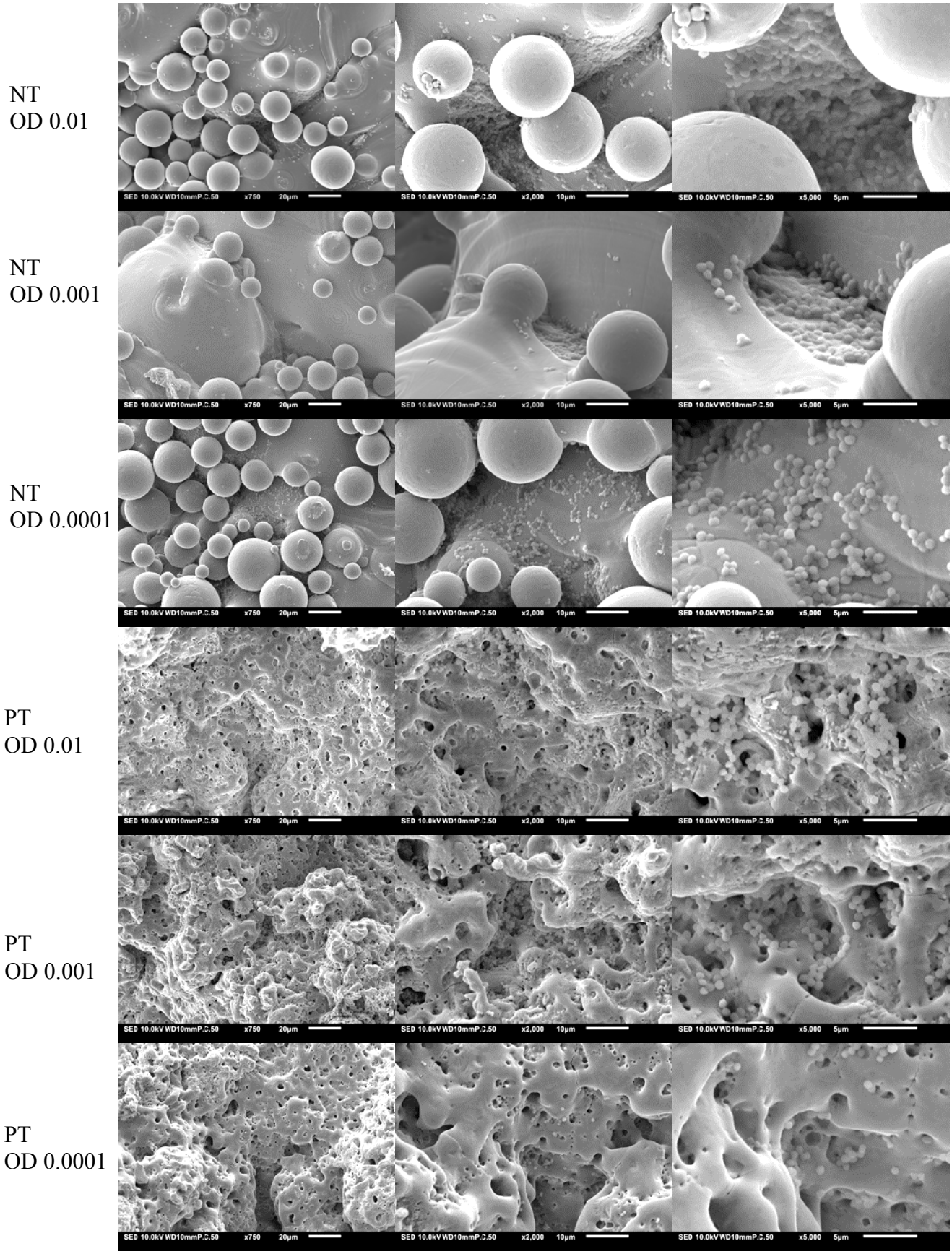

Figure 11: SEM images of adhering bacteria with different bacterial concentrations. The NT and PT implants (n=1) after 24h incubation with OD_{600} 0.01, 0.001 and 0.0001. Images representative for entire implant area.

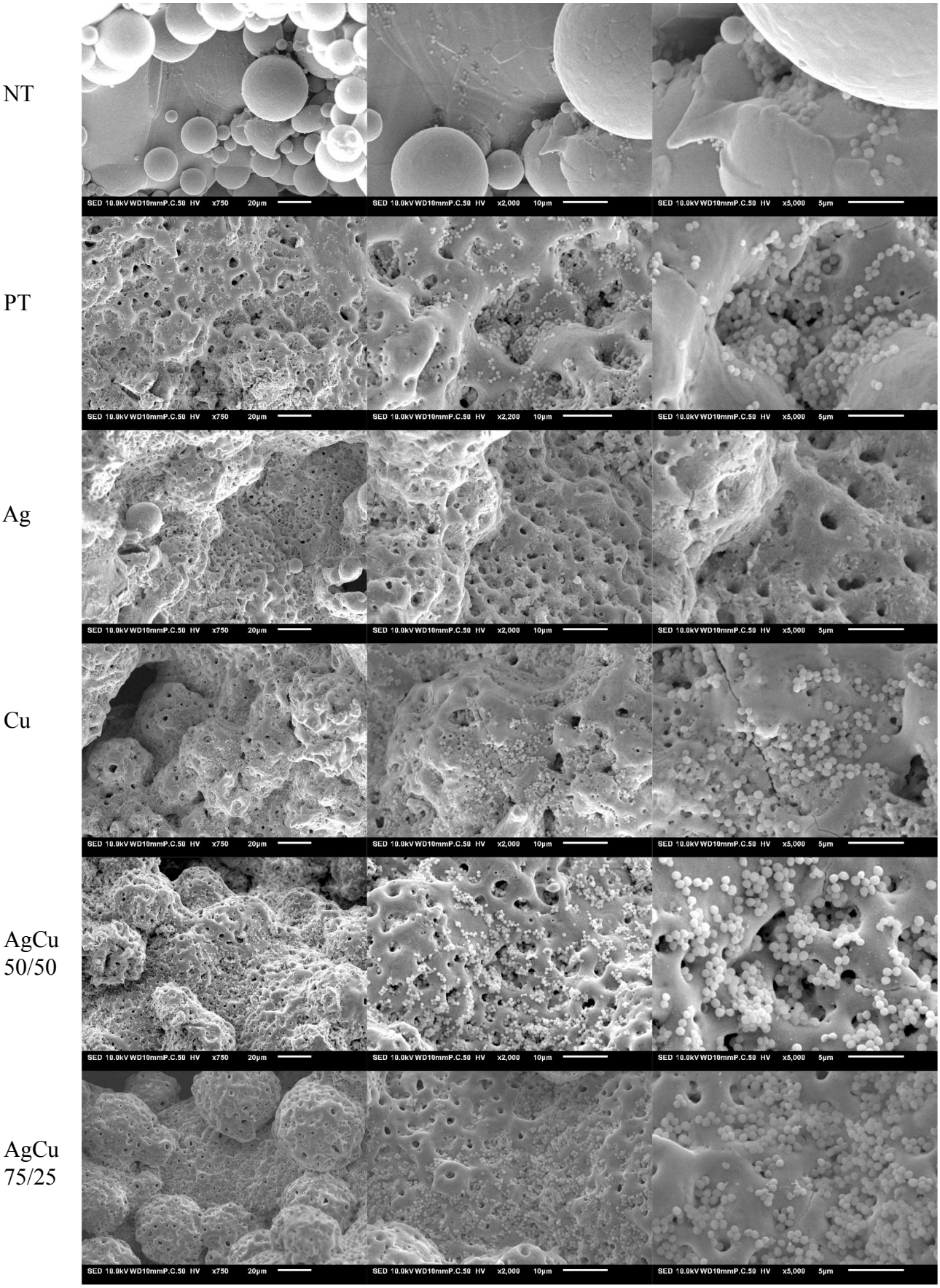

Figure 12: SEM images of adhering bacteria on implants. Representation of the adhering bacteria after the CFU assay for NT, PT, Ag, Cu, AgCu 50/50 and AgCu 75/25 (n=1) 24h. Images representative for entire implant area.

4 Discussion

The aim of this study was the synthesis, characterisation and antibacterial evaluation of Ag and Cu biofunctionalised self-defending Ti6Al4V implants. Implants were manufactured using an SLM printer. After removing Ti6Al4V powder particles from the implant surface, the surface was biofunctionalised using PEO with Ag and Cu NP. Using SEM characterisation, a layer of porous titanium oxide covering the titanium implants was observed (**Figure 3b-d**). As a result of the PEO, Ag and Cu NP were incorporated in the implant surface. The ratio of the incorporated Ag and Cu NP concurred with the initial Ag to Cu ratio in the electrolyte (**Figure 8**). Ag and Cu ion release measurements showed the implants expressing ion release for up to one month in PBS (**Figure 9c-d**). The combination of both Ag and Cu NP in the oxide layer showed an increase in Cu^{2+} release and a decrease in Ag^{+} release (**Figure 9a-b**).

Antibacterial evaluation with MRSA USA300 showed a large leaching activity for the implants containing a Ag, while the Cu implants showed limited leaching (**Figure 10a**). The combination implants showed comparable and lower leaching activity compared to the Ag implants, while the AgCu implant showed the largest leaching area. Based on a checkerboard assay, the MIC for Ag^{+} was 625 times lower compared to Cu^{2+} against MRSA. Combining Ag and Cu resulted in a decreasing MIC for both cations. CFU assay showed bacteria adhering on all implants and no non-adhering inhibition when incubated in 600µl TSB with 1% glucose, with a bacterial concentration of 6.5×10^{4} CFU/ml MRSA for 24h (**Figure 10b-e**). SEM characterisation confirmed the bacteria adhering on all but the Ag implants (**Figure 12**).

In the following sections, the obtained results are discussed, in order of appearance from the previous sections. Secondly, the value of this study is discussed and what type of follow up is required to further study the properties of Ag and Cu biofunctionalised titanium implants.

4.1 *Discussion of the results*

To compare the findings in this thesis with previous studies, he implant design was obtained from a previous study by I.A.J. van Hengel [46]. The implants were manufactured using SLMwhich has an increasing role in the production of orthopaedic implants. This additive manufacturing technique allows for the fast production of CAD based, patient specific implants, improving the compatibility of orthopaedic implants [48]. Therefore, the biofunctionalisation of the implants should be compatible with SLM manufactured implants.

Additive manufacturing and especially SLM, is mostly followed by post treatment, improving the mechanical properties and surface smoothness of the manufactured samples [48]. The mechanical properties of the implants were of no great influence on the research for the antibacterial properties of the implants, therefore all post treatment but powder removal was neglected in this study.

The biofunctionalised implant surfaces were synthesised using PEO. The process was monitored with the voltage response over time (**Figure 4**). The voltage response curves were compared by variables describing the four different sections; initial increase, dielectric breakdown, reduced voltage increase and final voltage. In this study, the sections and the variables describing the sections were defined with the following constraints. Firstly, the surface area of the implants was defined to be identical for all implants. Secondly, the duration of all sections was constant, independent of the experimental group. Finally, the gradients were the average gradient during the time intervals.

Within the PEO sections, the largest differences were obtained for the dielectric breakdown between PT and the combination groups and for the final voltage between the PT and all groups with NPs (**Figure 4**). Firstly, the dielectric breakdown was defined as the largest change in gradient. Dielectric breakdown is the rupture of the oxide layer. During the start of PEO, the oxide layer initially acts as a conductive isolation, with increasing isolative resistance

when progressing. When this oxide layer ruptures, a channel is formed, lowering local resistance at the rupture [52]. This results in a reduction of the resistance, reducing the voltage increase. This corresponds with the largest gradient reduction. However, the time steps used for measuring the voltage response are considerably large compared to the gradient of the initial voltage increase. Therefore, the differences in dielectric breakdown could reduce when a higher sample rate was used. Secondly, the final voltage was defined as the highest voltage during the measurement. The PT samples had a significantly higher voltage compared to the groups with NP. This could be explained by the increased conductivity of the electrolyte, by the addition of 3.0g/l NP. For better understanding of the PEO process, the conductivity of the electrolytes should be measured. When comparing to other articles, the same sections can be observed and the process variables are in the same range as S. Athanasiadis for the PT implants [49, 51, 61].

After the PEO process, the surface morphology of the implants was characterised. The titanium oxide surface-morphology was very similar for all PEO treated implants (**Figure 6**). The PEO treated titanium surface layer is characterised by circular micropores caused by local discharges distributed over the titanium oxide surface [51, 53]. Most studies on PEO treatment of Ti6Al4V are performed on solid flat surfaces, resulting in a smoother surface, with a uniform distribution of pores compared to the SLM printed implants in this study. For this study the long duration of the process, (300s) resulted in merging of pores. Together with the partly melted Ti6Al4V powder particles on the implant surface, PEO resulted in increased differences in height of the surface topology, different from other studies [1, 49-51]. Secondly, a low current density (1-6 A/dm^2 [49]) results in a grooved morphology, opposed to the deep, more circular pores as a result of the higher current (20 A/dm^2) density in this study [49-51, 62]. Based on the SEM characterisation and other studies with comparable parameters, there were no big differences in pore distribution, pore morphology and surface morphology of the obtained titanium oxide layer between the different experimental groups. Hence, the differences in the voltage response were not taken into account for the remaining of this study.

The incorporation of Ag and Cu NPs in the oxide layer occurs during the growth of the titanium oxide layer during PEO. The zeta potential measurements (**Figure 5a**) show that the zeta potential of the Ag (-16.8mV) and Cu NPs (-6.8mV) is negative. This indicates that the surfaces of the Ag and Cu NPs are negatively charged in the electrolyte. For the Ag NPs this could be explained by the Ag NP colloid chemical composition containing negative nitrate and chloride, resulting in the slightly greater negatively charged Ag NPs compared to Cu NPs [63]. Because of electrophoresis, caused by the applied electric field during PEO and the negative charge of the NPs, the NPs are attracted towards the anode, being the implant [56]. Sequentially the NPs are trapped in the growing layer and finally preserved during the successive growth [1].

Because of NP incorporation during the growth of the oxide layer, the incorporated NPs are located in open voids, in the outside layer or completely encapsulated by the oxide layer. The first two locations allow the NPs to release ions and supplement to the antibacterial activity of the implant. However, since the oxide layer grows during the bulk of the PEO process, most NPs are likely to be encapsulated in the oxide layer. Therefore, it is difficult to measure and control the amount of NP incorporated in the oxide layer that contribute to the antibacterial activity of the implant. Nonetheless, a trend was observed that indicated that an increasing amount of NP in the electrolyte resulted in an increase in ions released from the implant surface (**Figure 9:**). However, in the leaching activity of the Ag implants, this trend was marginally present (**Figure 10a**). The Ag implant had a slightly larger ZOI compared to Ag 75 (94%) and compared to Ag 50 (91%). The relation between the ion release and the leaching activity is related to the total amount of cations released as well as to the diffusion of the cations through the agar, which might affect the results. Therefore, the amount of NP in the electrolyte has limited influence on the ZOI assay.

In the chemical surface composition characterisation, Ag and Cu NP were found incorporated in the surface of the implants for all experimental groups (**Figure 7**). The combined Ag and Cu NP were not found as agglomerations on the implant surface, presumably by the continuous stirring of the electrolyte during the PEO [63]. The EDS spot analyses of the Ag and Cu NP (**Figure 7**) showed high quantities of Ag or Cu, but also elements from the neighbouring regions due to the inaccuracy of the analysis. In EDS analysis the X-ray spectrum emitted from a solid material is measured after bombarding it with a focused electron beam. The electron beam should be focused on a flat surface to retrieve the most accurate measurements but will still measure surrounding elements because of the focus diameter [64]. Due to the irregular surface of the oxide layer and the implant geometry, the focus area of the beam was never on a completely flat surface. Therefore, the spot analyses of the Ag and Cu NPs was inaccurate and obtaining other elements apart from the Ag and Cu. Therefore, a chemical intensity higher than 10% was defined as sufficient to confirm the presence of Ag or Cu NP.

For the Ag and Cu area ratio measurements, only the counts with a X-ray energy that described the Ag and Cu elements were taken into account (**Figure 8**). The presence of Ag and Cu NP was significantly lower compared to the other elements in the surface. This resulted in Ag and Cu to be filtered out by standard EDS software. The obtained measurements contained a large amount of noise caused by the roughness of the implant surface and other signal noise. To obtain a measurement of the Ag to Cu ratio on the implant surface, solely the Ag and Cu elements were taken into account. Due to the large amount of noise, the results had a large variance also showing the presence of Ag in the Cu implants and Cu in the Ag implants. Secondly the ratios could potentially deviate from the exact ratio present. To obtain a better indication of the Ag and Cu ratio on the surface, the oxide layer could be dissolved in sulphuric acid. The Ag and Cu in the dissolvent could be measured, indicating the present Ag to Cu ratio in the implant surface [1]. Nevertheless, the obtained ratios indicated a trend that was comparable to the ratio of Ag and Cu NPs in the electrolyte for each combination group.

When comparing these ratios to the ion release results, the ratio of NPs in the electrolyte corresponded to the Ag to Cu ratio in the ion release (**Figure 9:**). The ion release assay was performed with ICP-OES. This technique uses plasma and a spectrometer to measure the composition and concentration of elements in a solution [65]. ICP-OES measures the ions in the solution. However, before the analysis the samples were dissolved using HNO_3 to remove potential mass particles in the sample. Therefore, it is not definite that the measured ions are in ion state prior to the dissolution. However, the release kinetics of Ag in an aqueous solution is often described with the following stoichiometry reaction [36, 66, 67]:

$$4Ag_{(s)} + O_{2(aq)} + 4H^{+}{}_{(aq)} \longrightarrow 4Ag^{+}{}_{(aq)} 2H_2O_{(liq)}$$

The dissolution of Cu is similar except for the electron balance [68]:

$$2Cu_{(s)} + O_{2(aq)} + 4H^{+}{}_{(aq)} \longrightarrow 2Cu^{2+}{}_{(aq)} 2H_2O_{(liq)}$$

Assuming that the presence of oxygen and hydrogen during the assay was similar for all implants, a higher amount of either Ag or Cu present on the implant surface will result in a higher release of Ag^{+} or Cu^{2+}. This was observed for the implants with either Ag or Cu (**Figure 9**). However, for the implants containing both Ag and Cu, the Ag^{+} release was lower and Cu^{2+} release was higher compared to implants with the same amount of NP in the electrolyte. A potential cause is that combining Ag and Cu NP in the electrolyte results in an increased incorporation of Cu NP and decreased incorporation of Ag NP in the oxide layer. The Cu NP could intervene with the electrophoresis of the Ag NP towards the implant, during PEO. This could be measured by dissolving the oxide layer and measuring the Ag and Cu in the dissolved solution [1]. Another reasoning is that the combination of Ag and Cu on the implant surface

stimulated the release of Cu ions and inhibits the release of Ag ions. For the combination of Ag and Zn a similar almost double increase in Zn^{2+} and halved decrease in Ag^{+} release was observed when combined on titanium implants [69]. A similar micro galvanic coupling could be formed when combining Ag and Cu, according to the following redox reaction [70]:

$$Cu_{(s)} + 2Ag^{+}{}_{(aq)} + 2e^{-} \rightarrow Cu^{2+}{}_{(aq)} + 2Ag_{(s)} + 2e^{-}$$

Micro-galvanic couples are formed by the Ag and Cu NPs on the implant surface, making use of electron diffusion through the titanium [69, 71]. This reaction is initiated when the implants are introduced to the PBS. The oxidation of Cu results in the release of Cu^{2+} and the transfer of two electrons to the Ag NPs. Based on the surface characterisation, it was observed that the distance between Ag and Cu NP varied between 4μm and over 40μm (**Figure 7**). Because the distance between the Ag and Cu NPs varies, the distance could exceed the maximum distance that allows electron diffusion through the implant from Cu to Ag. Therefore, the ion release from the implant could result from the galvanic-coupling when the distance between the NPs allows electron transfer and individual Ag or Cu ion release kinetics when the distance is exceeded. This explains why the combination implants show both Ag and Cu ion release. To confirm these release mechanisms, follow up research on the interaction between Ag and Cu NPs in titanium oxide is required. Because it is a spontaneous redox reaction, this would result in electrical discharges along the implant surface. These electrical discharges could be measured by measuring the zeta potential along the surface of the implants in PBS [69].

The ion release determines for a large part the antibacterial leaching activity. The leaching assay (**Figure 10a**) showed that the addition of Cu NP present on the implant surface lowers the leaching activity of the implants. The Ag implants showed the highest leaching activity (1.12cm^2) while the Cu implant showed low leaching activity (0.16cm^2). This indicated that the presence of Ag on the implant had the largest contribution to the antibacterial activity of the implants. This could be explained by the MIC of Ag^{+}, which is a factor 625 lower compared to the MIC of Cu^{2+} against MRSA USA300. Although the Cu^{2+} MIC was considerably lower, the Cu^{2+} and Ag^{+} release from the implants was in the same range. The AgCu implant, that contained the same concentration Ag and Cu as for the solely Ag and Cu implants, showed the highest ZOI. This indicated that an increase in Ag and Cu present on the implant increases the leaching range. Higher concentrations of Ag and Cu in the electrolyte could potentially improve the ZOI even more. However, high quantities of Ag and Cu could also show cytotoxic effects therefore the increasing Ag and Cu should be assessed for cytotoxic effects. The cytotoxic effects of Cu NPs incorporated in titanium oxide layers have not been studied. However, the cytotoxic effects of Ag NPs incorporated in titanium oxide layers show high cytotoxic effects on with 3.0 g/l Ag NPs in the electrolyte [72], but also no signs of cytotoxicity on SLM implants [46]. Therefore, follow up research on the cytotoxic effects is required.

The checkerboard assay showed some lowering of the MIC for MRSA USA300 when Ag^{+} and Cu^{2+} were combined (**Section 3.3.2**). However, this combined effect was not substantial enough to improve the antibacterial efficiency of the implants during the antibacterial assays. The checkerboard assay showed reduction of the MIC with quantities of Cu^{2+} that was 625 times higher than released from the implants. Therefore, this concentration was not reached during the antibacterial assays and no synergy was obtained. The MIC values are dependent of the bacterial species and even bacterial strains [34, 73-75]. For this research the antibacterial assays were performed using MRSA USA300. Firstly, because *Staph. Aureus* is the most common cause for IAI [9]. Secondly, the methicillin resistance strain of *Staph. Aureus* has an increasing and dangerous occurrence [25]. Finally, the USA300 strain is able to form biofilms [76]. Therefore, the ability for the implants to inhibit growth of MRSA USA300 is relevant for clinical applicability.

The biofilm prevention assay demonstrated no significant differences between the biofunctionalised and non-biofunctionalised implants (**Figure 10b-d**). The leaching activity of the implants was insufficient to prevent the growth of non-adhering or planktonic bacteria in the incubation medium. Based on the ion release and MIC, this could be explained by the high concentration of CFU in the incubation medium, surpassing the leaching activity of the implants. Lowering the ratio between the volume of the incubation to the implant size, lowering the bacterial concentration or lowering the glucose in the medium might improve the activity.

The adhering CFU test showed no significant difference between the biofunctionalised and non-biofunctionalised implants. SEM imaging of the implants after the assay confirmed the presence of adhering bacteria on most implants apart from the Ag implant (**Figure 12**). The adhering bacteria on the NT implant were located between the transitions of the partly melted Ti6Al4V powder particles and the completely melted implant surface (**Figure 11** and **Figure 12a**). Therefore the adherence of bacteria is presumably higher for the porous NT implants compared to solid smooth titanium implants. Post treating the implants, by e.g. polishing might remove this effect. The PEO treated implants showed bacteria also adhering inside the pores. During the biofilm prevention assay the incubation medium was kept in motion, potentially causing fluid movements along the implant. The flowing might disturb the adhering of bacteria on the outside of the implant, where the flow is largest. In order to potentially observe prevention of adhering bacteria, lowering the number of bacteria in the medium or increasing the concentration of NPs in the electrolyte should be considered.

To sum up, the results indicate that PEO with the addition of Ag and Cu NPs allows the synthesis of Ag and Cu NP containing implant surfaces. The combination of Ag and Cu result in the increase of Cu^{2+} and decrease of Ag^{+} release from the implants, potentially resulting in weakening antibacterial activity against MRSA. To further asses the antibacterial potential of the Ag and Cu combination, follow up research on the Ag and Cu release kinetics, antibacterial assays with higher Ag and Cu NP concentrations are to be performed.

4.2 *Significance of study and recommendations*

This study showed the applicability of a technique to incorporate a combination of two different NPs. The appliance of PEO for the synthesis of the functionalized surface has advantages compared to other techniques. Firstly, it does not affect the macro porosity of the implant opposed to other techniques, e.g. loaded polymeric fiber coatings, that adhere a polymeric layer with antibacterial agents on the implant [77]. For the growth of the oxide layer, PEO requires titanium from the implant therefore the growth of the layer is accompanied by a sacrificial outside layer of the implant, resulting in a small increase of the implant thickness. Secondly, by adding calcium and phosphates in the electrolyte, osseointegration promoter HA can be formed in the oxide layer [46, 50, 61]. Thirdly, PEO improves the corrosion and weir resistance without affecting the bulk mechanical properties of the implants [44]. Finally, by adding NP in the electrolyte, these were incorporated in the oxide layer. So far this has been proven for Ag, Cu and Zn NP [46, 69]. Also the addition of strontium acetate in the electrolyte, resulted in the incorporation of strontium in the oxide layer [61]. This feature of PEO allows for an easy addition of one or more antibacterial agents in the oxide surface.

Apart from the antibacterial properties, other studies have shown osteogenic activity of Cu NPs [40, 78]. In order to assess this property of the Ag and Cu implants in this study, the cytotoxicity and viability of e.g. human mesenchymal stem cells (hMSC) on the implants should be measured [40]. The combination of Ag and Cu NPs could potentially use the antibacterial activity of the Ag NPs and the osteogenic activity of Cu NPs, similar to the combination of Ag and Sr [61]. Secondly, Cu is involved in the regulation of the expression of vascular endothelial growth factor (VEGF), a signal protein that stimulates vascular vessel maturation and formation

[78, 79]. This angiogenesis is important for bone ingrowth and repair, since it allows for the supply of minerals and disposing of waste products [80].

Apart from the antibacterial properties assessed in this study, the potential to combat antibacterial resistance and osteogenic properties need to be done. The combination of antibacterial agents is a promising approach for combatting the uprising resistant bacterial strains [81]. Antibacterial resistance is a dangerous phenomenon, resulting in many complications for the prevention and treatment of infections. Resistant bacteria have multiple mechanisms for defending themselves against antibacterial agents, including the efflux pumps, antibacterial neutralizing enzymes and changing antibacterial target groups [27, 32]. These mechanisms make it more difficult in treating infections with traditional antibacterial agents such as antibiotics [81]. The increasing use of antibiotics, give rise to bacterial strains that are resistant to these antibiotics. In addition, bacteria causing IAI have resistant strains, such as MRSA [25]. Therefore, the development and application of new agents is of the essence. Both the antibacterial mechanisms of metallic nanomaterials and the combination of multiple antibacterial mechanisms has shown potential [30, 81]. Metallic nanomaterials have two main antibacterial mechanisms. Firstly, they secrete toxic cations, Ag^{+} and Cu^{2+} that bind to the negatively charged cell walls of the bacteria, causing rapture of the cell walls and cell death. Secondly, they induce oxidative stress in bacterial cell membranes by the formation of reactive oxygen species (ROS) [38, 82, 83]. So far, there were limited reports of bacteria that showed resistance for metallic nanomaterials or cations [16, 84]. Apart from the novel antibacterial mechanisms of the individual agents, the application of multiple agents used simultaneously combats resistance in two ways. Firstly, the dual mechanism allows one mechanism to take over when bacteria show resistance towards the other. Therefore, the combination prevents the propagation of resistant strains towards either antibacterial mechanism while also killing more strains compared to single agents. Secondly, one agent could restore the antibacterial efficiency of the other by disrupting the resistance mechanism [81]. Ag and Cu NP incorporated in the oxide layer, release cations with different charges potentially having different antibacterial properties[84], but also potentially create ROS and subsequently oxidative stress in bacteria close to the surface of the implant. These combined mechanisms may result in effective targeting of resistant bacteria.

The release of Ag^{+} and Cu^{2+} from the implant surface needs to be tuned to maximize the antibacterial activity, while remaining limiting the cytotoxic effects. During surgery, a larger area around the implant is damaged and has a larger potential to be infected. Although minimally invasive surgeries are emerging, it is inevitable to damage tissue around the implant. After surgery these tissue are at risk to be infected [85]. The release of antibacterial cations from the surface also defends the tissue around the implant from infections. Interstitial fluids transport the ions away from the implant, to potential distal infected areas. Apart from the toxic dangers of wandering cations, fluid movement also lowers the local dosage of ions. Since the main cause for IAI were biofilms, the local dosage of the antibacterial agents should be sufficient until the surgical incision is healed. This is approximately 3 months after surgery [5]. The implants in this study were tested up to one month and showed substantial ion over that time period *in vitro*. The ion release dosage of a 15mm implant was not sufficient to reach the MIC. However, a large implant has more surface area potential for more NP, most likely reaching the MIC. Therefore, follow up research with a lower concentration of bacteria or larger implants should be assessed.

Apart from the antibacterial properties of Ag and Cu ions and NP, cytotoxicity should be prevented. Oxidative stress and cytotoxicity are serious dangers of using NP [86]. However, firstly the toxic effects of roaming NP may be prevented by the incorporation of the NP in the oxide layer [84]. The NPs are strongly fixated in the oxide layer. Therefore, the NPs remain in the implant and restrain the toxic and antibacterial activity near the implant. Secondly, the ROS

formation could be treated by additional antioxidant treatment [87]. Finally, local prophylaxis increases the local dosage of antimicrobial agents. This allows for the total dosage to be lower compared to systemic prophylaxis [17].

In previous studies the antibacterial activity of Ag and Cu was combined with osteogenic and angiogenesis properties of HA and Cu. Firstly, the addition of calcium acetate and glycerophosphate in electrolyte during PEO, resulted in the formation of HA on the implant surface [46, 61]. HA is known to have osteogenic properties, promoting bone formation [45]. Secondly, ionic Cu has shown both osteogenesis and angiogenesis promotion [40, 79]. These cell-promoting properties could improve the bone formation around the implant, reducing the time period for infection and biofilm formation on the implants. Follow up research on the cell viability and adherence of e.g. hMSC on the Ag and Cu containing implants, indicates osteogenic activity, while the increase in release of VEGF indicates promotion of angiogenesis.

Altogether, the results of this study showed the feasibility to incorporate both Ag and Cu NPs in PEO treated titanium implant surfaces. To further assess the potential of the combination of Ag and Cu NPs for biofilm prevention, osteogenic promotion and combatting of resistant bacteria, follow up research is required. New antibacterial approaches are required to combat the rise of resistant bacteria. The rise in demand for implants increases the urgency for dealing with IAI. By combining the high antibacterial properties of Ag NPs and potential dual functioning Cu NPs, fixated in the implant surface, these self-defending implants decrease the chances for IAI, potentially improve bone ingrowth and will have a longterm applicability for the combat against resistant bacteria.

5 Conclusions

In this study, additively manufactured, porous Ti6Al4V implants were biofunctionalised with PEO to incorporate Ag and Cu NPs in the implant surface. By varying the Ag to Cu ratio and amount of NPs in the electrolyte, the amount and ratio of incorporated NP could be determined. The combination of Ag and Cu NPs on the implants showed an increased cumulative release of Cu^{2+} and decreased release of Ag^{+} from the implant surface for at least 1 month *in vitro*. Furthermore, the antibacterial biofunctionalised implants showed antibacterial leaching activity for all implants with the largest leaching zone for the implant with the highest Ag and Cu concentration. Furthermore, the biofunctionalised implants did not prevent bacterial adhesion or killing of planktonic bacteria in the applied antibacterial tests. Therefore, antibacterial assays need to be optimised. Overall PEO is a technique that shows much promise due to its possibility to simultaneously incorporate multiple NPs. The combination of Ag and Cu NPs requires further research to evaluate their full potential to prevent IAI.

6 Acknowledgements

Hereby I would like to thank all people that supported me during this thesis. First of all, I would like to thank ir. Ingmar van Hengel who supported me on a daily basis. He was always prepared to discuss findings, while pushing me to stay critical on my own findings and those of others. Apart from that, he taught me how to present my findings in a more scientific manner, which is much appreciated. Secondly, I would like to thank dr. ir. Iulian Apachitei for sharing his wide knowledge on biomaterials and always finding time to give the feedback I need on both my research and my thesis despite his busy schedule. Next, I would like to thank prof. dr. Amir Zadpoor for his support during my thesis and introducing me to this study I enjoyed working on. Furthermore, I would like to thank Sander Leeflang for all his support in and around the Biolab and on the production of the multi holder that made the production of the implants much easier. I would also like to thank Michel van den Brink for the ICP-OES measurements and teaching me more about the process.

Furthermore, the antibacterial assays were performed in the Microbiology lab in the UMC Utrecht. Thanks to Ad Fluit for making this collaboration possible. Secondly, I would like to thank Barry Benaissa-Trouw for her enthusiasm and allowing us to make use of her incredible pipetting skills. Thanks to Nico and Melissa for helping me with several tests. Thanks to Marnix for providing me with some chemistry knowledge. Finally, I would like to thank Dinko, Hester, Daria, Enzo and Julie for allowing me to pitch my findings and broadening my vision on the subject.

7 References

1. Necula, B.S., *Silver-based antibacterial surfaces for bone implants*, in *Biomaterials and Tissue Biomechanics*. 2013, TU Delft: TU Delft Database.
2. Klevens, R.M., et al., *Estimating health care-associated infections and deaths in US hospitals, 2002.* Public health reports, 2007. **122**(2): p. 160-166.
3. Weinstein, R.A. and R.O. Darouiche, *Device-associated infections: a macroproblem that starts with microadherence.* Clinical Infectious Diseases, 2001. **33**(9): p. 1567-1572.
4. Cloutier, M., D. Mantovani, and F. Rosei, *Antibacterial coatings: challenges, perspectives, and opportunities.* Trends in biotechnology, 2015. **33**(11): p. 637-652.
5. Berry, D.J., *Third AJRR Annual Report on Hip and Knee Arthroplasty Data*. 2016, American Joint Replacement Registry.
6. Fingar, K.R., et al., *Most frequent operating room procedures performed in US hospitals, 2003–2012: statistical brief# 186.* 2006.
7. Geetha, M., et al., *Ti based biomaterials, the ultimate choice for orthopaedic implants–a review.* Progress in materials science, 2009. **54**(3): p. 397-425.
8. Campoccia, D., L. Montanaro, and C.R. Arciola, *The significance of infection related to orthopedic devices and issues of antibiotic resistance.* Biomaterials, 2006. **27**(11): p. 2331-2339.
9. Montanaro, L., et al., *Scenery of Staphylococcus implant infections in orthopedics.* Future microbiology, 2011. **6**(11): p. 1329-1349.
10. Davies, D., *Understanding biofilm resistance to antibacterial agents.* Nature reviews Drug discovery, 2003. **2**(2): p. 114.
11. Donlan, R.M., *Biofilms and device-associated infections.* Emerging infectious diseases, 2001. **7**(2): p. 277.
12. Ceri, H., et al., *The Calgary Biofilm Device: new technology for rapid determination of antibiotic susceptibilities of bacterial biofilms.* Journal of clinical microbiology, 1999. **37**(6): p. 1771-1776.
13. Arciola, C.R., et al., *Biofilm-based implant infections in orthopaedics*, in *Biofilm-based healthcare-associated infections*. 2015, Springer. p. 29-46.
14. Römling, U. and C. Balsalobre, *Biofilm infections, their resilience to therapy and innovative treatment strategies.* Journal of internal medicine, 2012. **272**(6): p. 541-561.
15. Trampuz, A. and W. Zimmerli, *Diagnosis and treatment of implant-associated septic arthritis and osteomyelitis.* Current infectious disease reports, 2008. **10**(5): p. 394-403.
16. Kurtz, S., et al., *Prevalence of primary and revision total hip and knee arthroplasty in the United States from 1990 through 2002.* JBJS, 2005. **87**(7): p. 1487-1497.
17. Darouiche, R.O., *Antimicrobial approaches for preventing infections associated with surgical implants.* Clinical infectious diseases, 2003. **36**(10): p. 1284-1289.
18. Pittet, D., et al., *The World Health Organization guidelines on hand hygiene in health care and their consensus recommendations.* Infection Control & Hospital Epidemiology, 2009. **30**(7): p. 611-622.
19. Dumville, J.C., et al., *Preoperative skin antiseptics for preventing surgical wound infections after clean surgery.* Cochrane Database Syst Rev, 2013. **3**(3).
20. Espehaug, B., et al., *Antibiotic prophylaxis in total hip arthroplasty: review of 10 905 primary cemented total hip replacements reported to the Norwegian arthroplasty register, 1987 to 1995.* The Journal of bone and joint surgery. British volume, 1997. **79**(4): p. 590-595.
21. Cavanaugh, D.L., et al., *Better prophylaxis against surgical site infection with local as well as systemic antibiotics: an in vivo study.* The Journal of Bone and Joint Surgery. American volume., 2009. **91**(8): p. 1907.
22. Halpern, L.R. and T.B. Dodson, *Does prophylactic administration of systemic antibiotics prevent postoperative inflammatory complications after third molar surgery?* Journal of Oral and Maxillofacial Surgery, 2007. **65**(2): p. 177-185.

23. Control, C.f.D. and Prevention, *Antibiotic resistance threats in the United States, 2013*. 2013: Centres for Disease Control and Prevention, US Department of Health and Human Services.
24. Akimitsu, N., et al., *Increase in resistance of methicillin-resistant Staphylococcus aureus to β-lactams caused by mutations conferring resistance to benzalkonium chloride, a disinfectant widely used in hospitals.* Antimicrobial agents and chemotherapy, 1999. **43**(12): p. 3042-3043.
25. Hiramatsu, K., *Molecular evolution of MRSA.* Microbiology and immunology, 1995. **39**(8): p. 531-543.
26. Livermore, D.M., *Bacterial resistance: origins, epidemiology, and impact.* Clinical infectious diseases, 2003. **36**(Supplement_1): p. S11-S23.
27. Kalan, L. and G.D. Wright, *Antibiotic adjuvants: multicomponent anti-infective strategies.* Expert reviews in molecular medicine, 2011. **13**.
28. Heinemann, J.A., R.G. Ankenbauer, and C.F. Amábile-Cuevas, *Do antibiotics maintain antibiotic resistance?* Drug discovery today, 2000. **5**(5): p. 195-204.
29. Levy, S.B., *The challenge of antibiotic resistance.* Scientific American, 1998. **278**(3): p. 46-53.
30. Pelgrift, R.Y. and A.J. Friedman, *Nanotechnology as a therapeutic tool to combat microbial resistance.* Advanced drug delivery reviews, 2013. **65**(13-14): p. 1803-1815.
31. Demerec, M., *Origin of bacterial resistance to antibiotics.* Journal of bacteriology, 1948. **56**(1): p. 63.
32. Sun, J., Z. Deng, and A. Yan, *Bacterial multidrug efflux pumps: mechanisms, physiology and pharmacological exploitations.* Biochemical and biophysical research communications, 2014. **453**(2): p. 254-267.
33. Marquez, B., *Bacterial efflux systems and efflux pumps inhibitors.* Biochimie, 2005. **87**(12): p. 1137-1147.
34. Garza-Cervantes, J.A., et al., *Synergistic Antimicrobial Effects of Silver/Transition-metal Combinatorial Treatments.* Scientific Reports, 2017. **7**(1): p. 903.
35. Raghunath, A. and E. Perumal, *Metal oxide nanoparticles as antimicrobial agents: a promise for the future.* International journal of antimicrobial agents, 2017. **49**(2): p. 137-152.
36. Loza, K., et al., *The dissolution and biological effects of silver nanoparticles in biological media.* Journal of Materials Chemistry B, 2014. **2**(12): p. 1634-1643.
37. Ruparelia, J.P., et al., *Strain specificity in antimicrobial activity of silver and copper nanoparticles.* Acta biomaterialia, 2008. **4**(3): p. 707-716.
38. Dizaj, S.M., et al., *Antimicrobial activity of the metals and metal oxide nanoparticles.* Materials Science and Engineering: C, 2014. **44**: p. 278-284.
39. Ramyadevi, J., et al., *Synthesis and antimicrobial activity of copper nanoparticles.* Materials letters, 2012. **71**: p. 114-116.
40. Burghardt, I., et al., *A dual function of copper in designing regenerative implants.* Biomaterials, 2015. **44**: p. 36-44.
41. Biswas, P. and R. Bandyopadhyaya, *Synergistic antibacterial activity of a combination of silver and copper nanoparticle impregnated activated carbon for water disinfection.* Environmental Science: Nano, 2017. **4**(12): p. 2405-2417.
42. JankauskaitĿ, V., et al., *Bactericidal effect of graphene oxide/Cu/Ag nanoderivatives against Escherichia coli, Pseudomonas aeruginosa, Klebsiella pneumoniae, Staphylococcus aureus and Methicillin-resistant Staphylococcus aureus.* International journal of pharmaceutics, 2016. **511**(1): p. 90-97.
43. Valodkar, M., et al., *Synthesis and anti-bacterial activity of Cu, Ag and Cu–Ag alloy nanoparticles: a green approach.* Materials Research Bulletin, 2011. **46**(3): p. 384-389.

44. Karaji, Z.G., et al., *Effects of plasma electrolytic oxidation process on the mechanical properties of additively manufactured porous biomaterials.* Materials Science and Engineering: C, 2017. **76**: p. 406-416.
45. Lugovskoy, A. and S. Lugovskoy, *Production of hydroxyapatite layers on the plasma electrolytically oxidized surface of titanium alloys.* Materials Science and Engineering: C, 2014. **43**: p. 527-532.
46. van Hengel, I.A., et al., *Selective laser melting porous metallic implants with immobilized silver nanoparticles kill and prevent biofilm formation by methicillin-resistant Staphylococcus aureus.* Biomaterials, 2017. **140**: p. 1-15.
47. Taniguchi, N., et al., *Effect of pore size on bone ingrowth into porous titanium implants fabricated by additive manufacturing: an in vivo experiment.* Materials Science and Engineering: C, 2016. **59**: p. 690-701.
48. Gibson, I., D.W. Rosen, and B. Stucker, *Sheet Lamination Processes*, in *Additive Manufacturing Technologies*. 2010, Springer. p. 223-252.
49. Nabavi, H.F., M. Aliofkhazraei, and A.S. Rouhaghdam, *Morphology and corrosion resistance of hybrid plasma electrolytic oxidation on CP-Ti.* Surface and Coatings Technology, 2017. **322**: p. 59-69.
50. Yerokhin, A., et al., *Plasma electrolysis for surface engineering.* Surface and coatings technology, 1999. **122**(2-3): p. 73-93.
51. Cheng, Y., et al., *A comparison of plasma electrolytic oxidation of Ti-6Al-4V and Zircaloy-2 alloys in a silicate-hexametaphosphate electrolyte.* Electrochimica Acta, 2015. **165**: p. 301-313.
52. KANPUR, I., *Dielectric breakdown*. 2012: NPTEL website.
53. Wheeler, J., et al., *Evaluation of micromechanical behaviour of plasma electrolytic oxidation (PEO) coatings on Ti–6Al–4V.* Surface and Coatings Technology, 2010. **204**(21-22): p. 3399-3409.
54. Information, N.C.f.B. *Calcium Acetate Hydrate, ReagentPlus(R), >=99% (Titration), Powder*. May 14, 2018]; Available from: https://pubchem.ncbi.nlm.nih.gov/substance/24892291.
55. Information, N.C.f.B. *Calcium Glycerophosphate*. accessed May 14, 2018]; Available from: https://pubchem.ncbi.nlm.nih.gov/compound/120096.
56. Instruments, M., *Zetasizer Nano Series User Manual*. 2005.
57. AB, M., *Phosphate Buffered Saline (PBS), pH 7.4 and 7.2*. 2010.
58. Paul R. Gaines, P., *A Guide for using ICP-OES and ICP-MS*, in *ICP Operations Guide*, I. Inorganic Ventures, Editor. 2011.
59. Wang, J., et al., *Silver-nanoparticles-modified biomaterial surface resistant to staphylococcus: new insight into the antimicrobial action of silver.* Scientific reports, 2016. **6**: p. 32699.
60. Carrel, M., E.N. Perencevich, and M.Z. David, *USA300 methicillin-resistant Staphylococcus aureus, United States, 2000–2013.* Emerging infectious diseases, 2015. **21**(11): p. 1973.
61. Athanasiadis, S., *Osteogenic and antibacterial acitivty of strontium and silver containing additively manufactured titanium implants.*, in *Biomedical Engineering*. 2016, TU-Delft: Delft.
62. Nabavi, H.F., M. Aliofkhazraei, and A.S. Rouhaghdam, *Electrical characteristics and discharge properties of hybrid plasma electrolytic oxidation on titanium.* Journal of Alloys and Compounds, 2017. **728**: p. 464-475.
63. Kim, J.S., et al., *Antimicrobial effects of silver nanoparticles.* Nanomedicine: Nanotechnology, Biology and Medicine, 2007. **3**(1): p. 95-101.
64. Goldstein, J.I., et al., *Scanning electron microscopy and X-ray microanalysis*. 2017: Springer.

65. Hitachi. *Principle of ICP Optical Emission Spectrometry (ICP-OES)*. 2018 [cited 2018 20-3-2018]; Available from: https://www.hitachi-hightech.com/global/products/science/tech/ana/icp/descriptions/icp-oes.html.
66. Lee, Y.J., et al., *Ion-release kinetics and ecotoxicity effects of silver nanoparticles.* Environmental toxicology and chemistry, 2012. **31**(1): p. 155-159.
67. Liu, J. and R.H. Hurt, *Ion release kinetics and particle persistence in aqueous nano-silver colloids.* Environmental science & technology, 2010. **44**(6): p. 2169-2175.
68. Lu, B.C.-Y. and W. Graydon, *THE RATE OF DISSOLUTION OF COPPER.* Canadian Journal of Chemistry, 1954. **32**(2): p. 153-163.
69. Jin, G., et al., *Synergistic effects of dual Zn/Ag ion implantation in osteogenic activity and antibacterial ability of titanium.* Biomaterials, 2014. **35**(27): p. 7699-7713.
70. Shodor. *Redox Reactions*. 2008 [cited 2018; Available from: http://www.shodor.org/unchem/advanced/redox/.
71. Cao, H.L., et al., *Biological actions of silver nanoparticles embedded in titanium controlled by micro-galvanic effects.* Biomaterials, 2011. **32**(3): p. 693-705.
72. Necula, B., et al., *In vitro cytotoxicity evaluation of porous TiO2–Ag antibacterial coatings for human fetal osteoblasts.* Acta biomaterialia, 2012. **8**(11): p. 4191-4197.
73. Bakhshandeh, S., et al., *Simultaneous Delivery of Multiple Antibacterial Agents from Additively Manufactured Porous Biomaterials to Fully Eradicate Planktonic and Adherent Staphylococcus aureus.* ACS applied materials & interfaces, 2017. **9**(31): p. 25691-25699.
74. Du, W.-L., et al., *Antibacterial activity of chitosan tripolyphosphate nanoparticles loaded with various metal ions.* Carbohydrate Polymers, 2009. **75**(3): p. 385-389.
75. Berger, T., et al., *Electrically generated silver ions: quantitative effects on bacterial and mammalian cells.* Antimicrobial Agents and Chemotherapy, 1976. **9**(2): p. 357.
76. McCarthy, H., et al., *Methicillin resistance and the biofilm phenotype in Staphylococcus aureus.* Frontiers in cellular and infection microbiology, 2015. **5**: p. 1.
77. Ashbaugh, A.G., et al., *Polymeric nanofiber coating with tunable combinatorial antibiotic delivery prevents biofilm-associated infection in vivo.* Proceedings of the National Academy of Sciences, 2016. **113**(45): p. E6919-E6928.
78. Xie, H. and Y.J. Kang, *Role of copper in angiogenesis and its medicinal implications.* Current medicinal chemistry, 2009. **16**(10): p. 1304-1314.
79. Wu, C., et al., *Copper-containing mesoporous bioactive glass scaffolds with multifunctional properties of angiogenesis capacity, osteostimulation and antibacterial activity.* Biomaterials, 2013. **34**(2): p. 422-433.
80. Carano, R.A. and E.H. Filvaroff, *Angiogenesis and bone repair.* Drug discovery today, 2003. **8**(21): p. 980-989.
81. Khameneh, B., et al., *Breakthroughs in bacterial resistance mechanisms and the potential ways to combat them.* Microbial pathogenesis, 2016. **95**: p. 32-42.
82. Zhang, W., et al., *Photogeneration of reactive oxygen species on uncoated silver, gold, nickel, and silicon nanoparticles and their antibacterial effects.* Langmuir, 2013. **29**(15): p. 4647-4651.
83. Vimbela, G.V., et al., *Antibacterial properties and toxicity from metallic nanomaterials.* International journal of nanomedicine, 2017. **12**: p. 3941.
84. Knetsch, M.L. and L.H. Koole, *New strategies in the development of antimicrobial coatings: the example of increasing usage of silver and silver nanoparticles.* Polymers, 2011. **3**(1): p. 340-366.
85. Mazuski, J.E., et al., *The Surgical Infection Society guidelines on antimicrobial therapy for intra-abdominal infections: an executive summary.* Surgical Infections, 2002. **3**(3): p. 161-173.
86. Johnston, H.J., et al., *A review of the in vivo and in vitro toxicity of silver and gold particulates: particle attributes and biological mechanisms responsible for the observed toxicity.* Critical reviews in toxicology, 2010. **40**(4): p. 328-346.

87. Mittler, R., *Oxidative stress, antioxidants and stress tolerance.* Trends in plant science, 2002. **7**(9): p. 405-410.

8 Appendices

A. PEO set-up

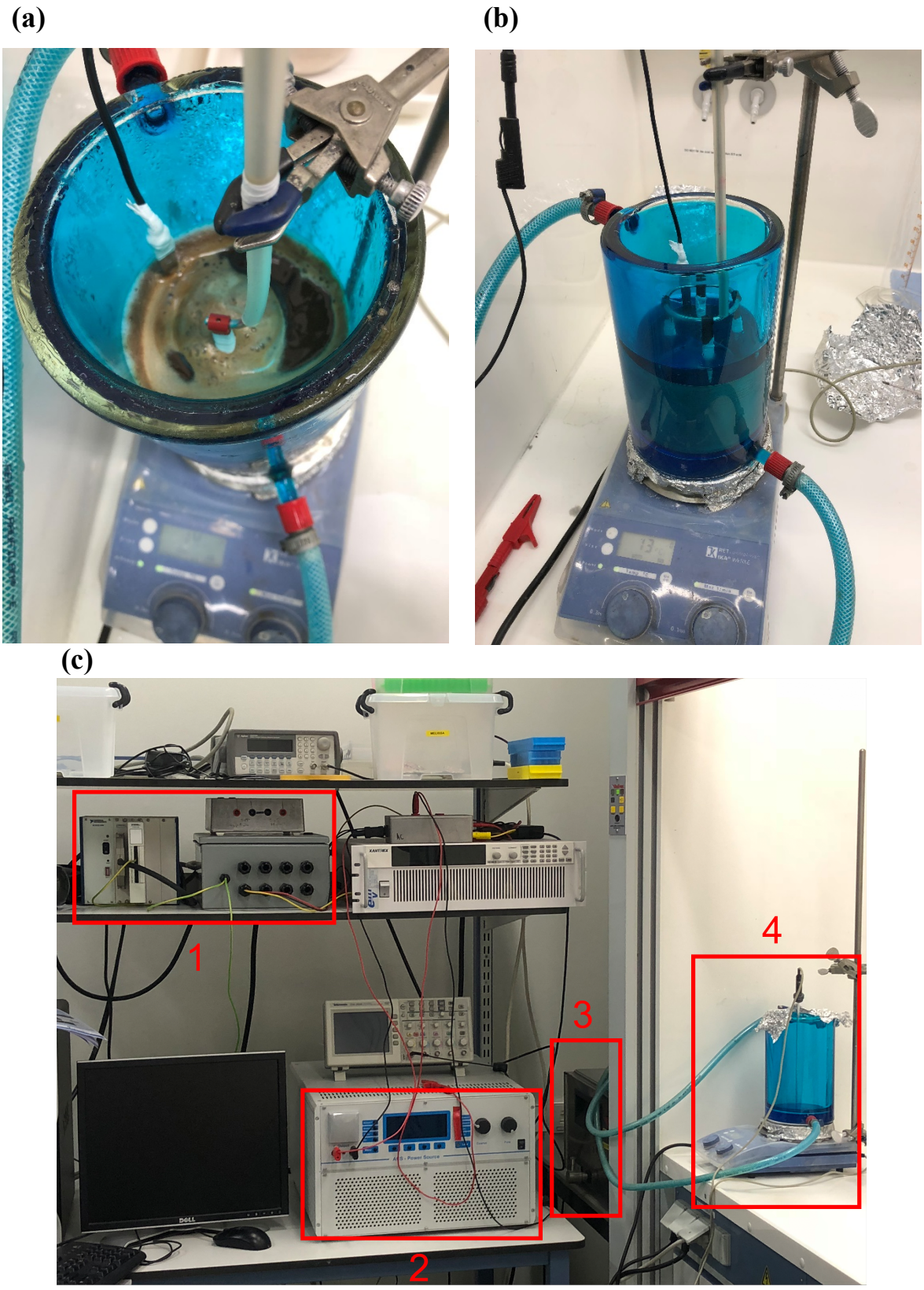

Figure 13: The PEO set-up used. A) The cooled electrolytic cell, with single sample holder. B) The electrolytic cell on the stirring machine. C) The PEO set-up showing (1) the data acquisition (2) the AC power source (3) thermostatic bath (4) the electrolytic cell with magnetic stirrer

B. Multi-holder

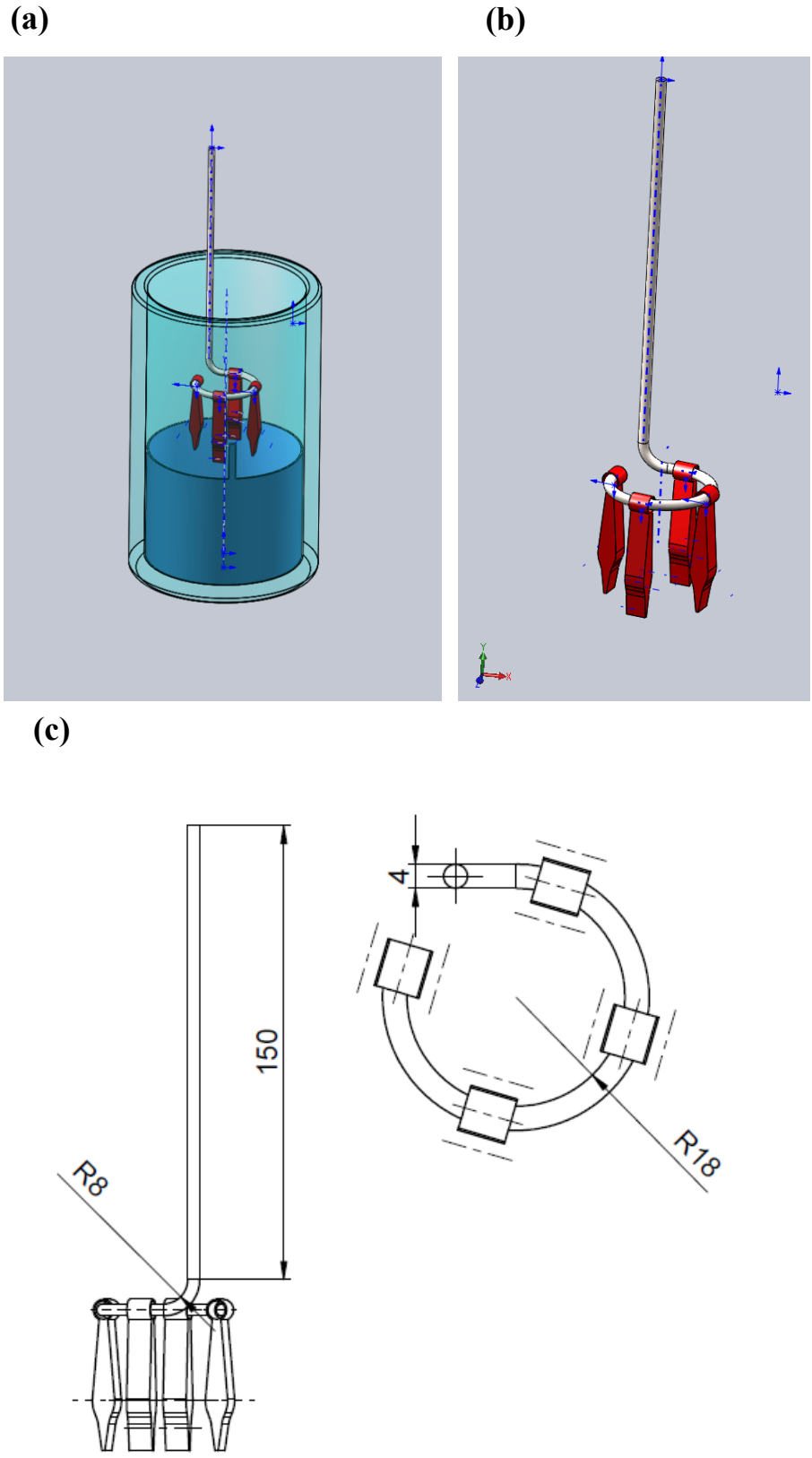

Figure 14: Multi holder design and schematics. a) solidworks design of the multiholder within the electrolytic cell. b) solidworks design of the multiholder with four clamps, positioned perpendicular to each other to improve the position of the implants during PEO. c) The schematics of the multi holder used to produce the holder.

(a) (b)

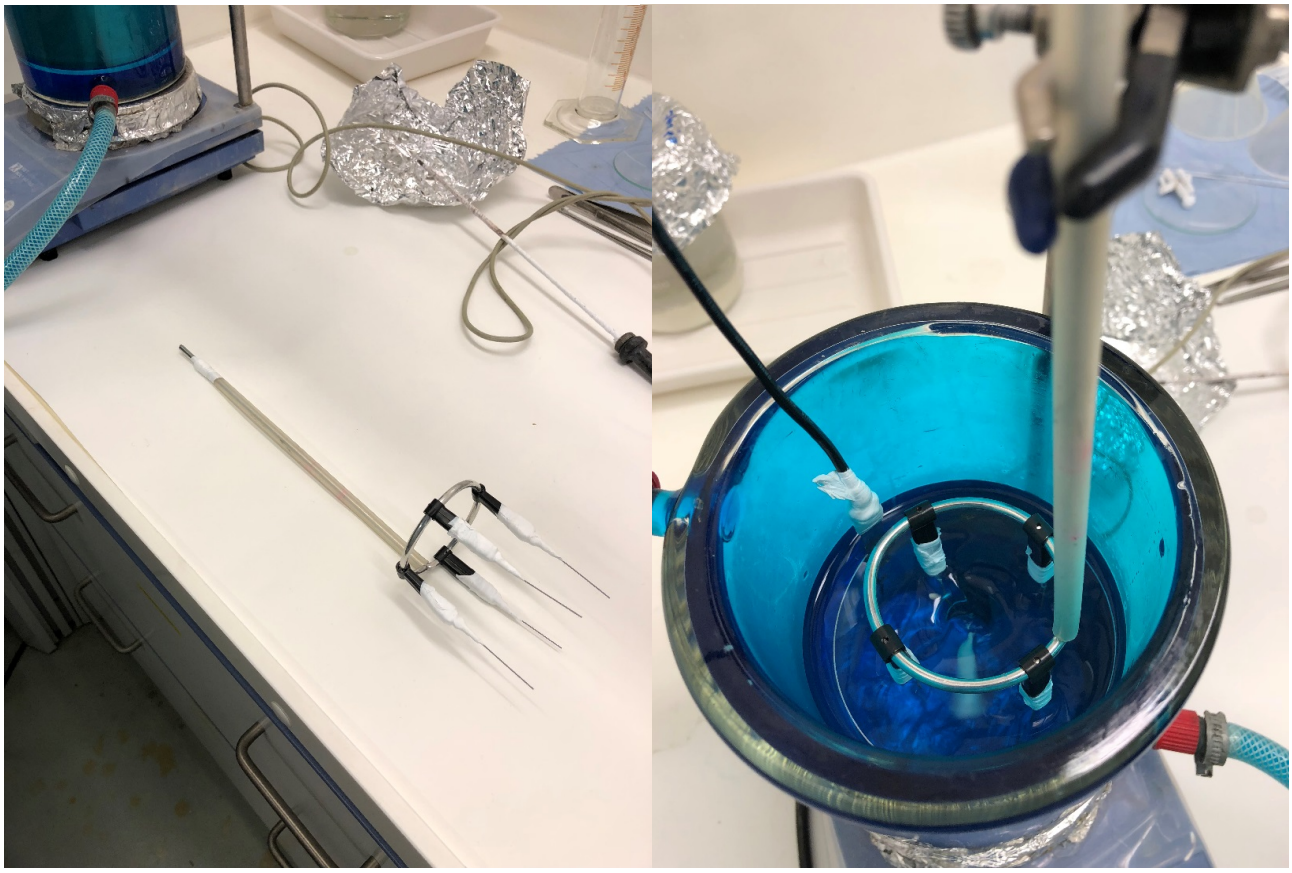

Figure 15 Multi holder with implants. a) showing the finished multi holder, with four implants isolated using isolation tape. b) the multi holder positioned in the centre of the electrolytic cell, indicated by the vortex as result of the stirring of the electrolyte.

The implants were interconnected in a parallel circuit, resulting in an increase in current required and a similar response voltage, compared to the single implant samples. The current used for one implant was 0.390mA while the current for four implants was 1.560A. The graph in **Figure 16** shows the average voltage response for the single implant measurements with the average response of the holder with four samples. The average error over the entire measurement for the multi sample holder is ±3.4V, while that of the single sample holder is ±3.1V. The multi sample holder shows less saturation approaching the end. The average final voltages for the multi sample holder (242V) and single samples holder (246V) are comparable. The voltage response was very similar; hence the multi-holder was used for the final implants.

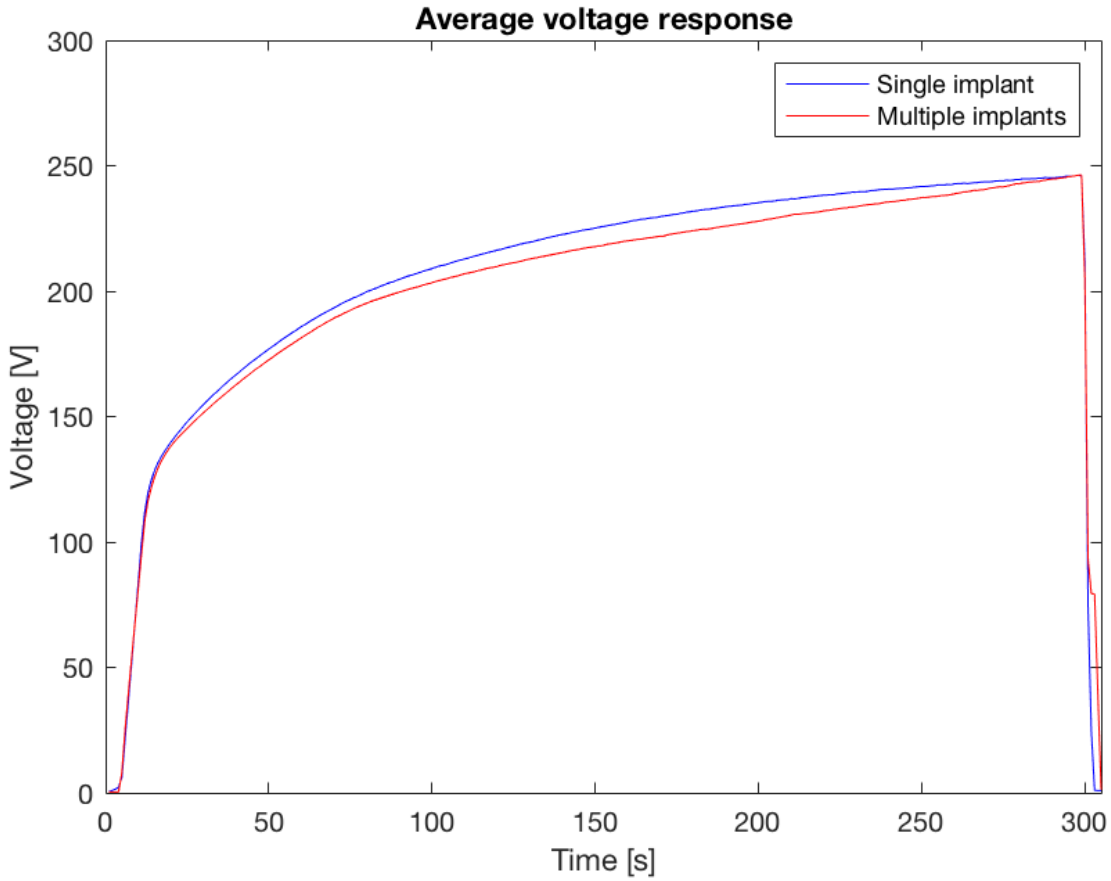

Figure 16: Single and multiple implants PEO voltage response. The averaged voltage response curve over time for both single implants and four implants. The average error over the entire measurement for the multi sample holder is ±3.4V, while that of the single sample holder is ±3.1V. The multi sample holder shows less saturation approaching the end. The average final voltages for the multi sample holder (242V) and single samples holder (246V) are comparable.

C. Ratio images

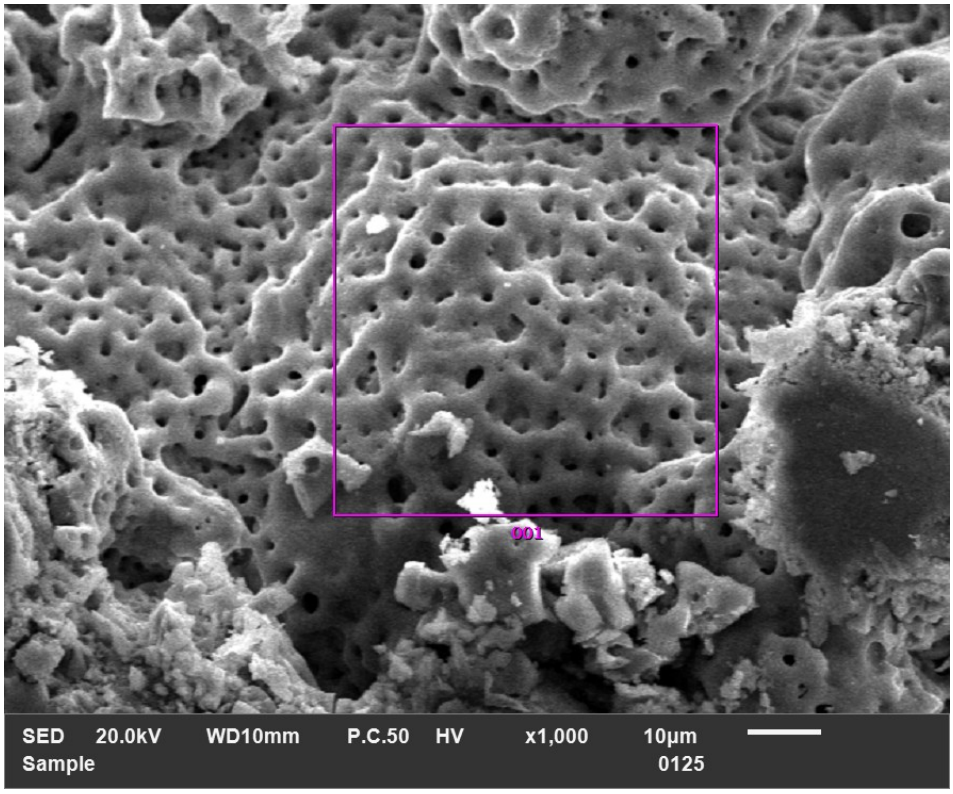

Figure 17 Ratio EDS area measurement of an AgCu 25/75 implant. The purple square indicates the analysis area used to measure the ratio between Ag and Cu present in that area. For this measurement, the obtained ratio was 25.39% Ag and 74.61% Cu.

D. Zone of inhibition

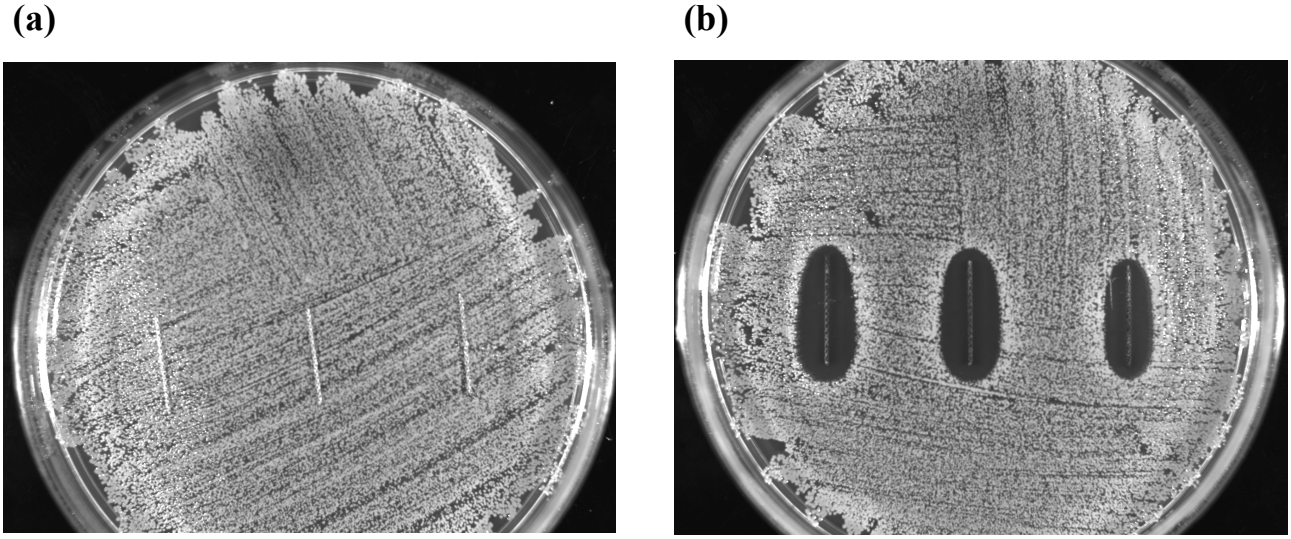

Figure 18: Leaching assay for NT and AgCu 100/100. A) The NT implants showing no ZOI, B) The AgCu 100/100 implants showing a clear ZOI.

E. Checkerboard results

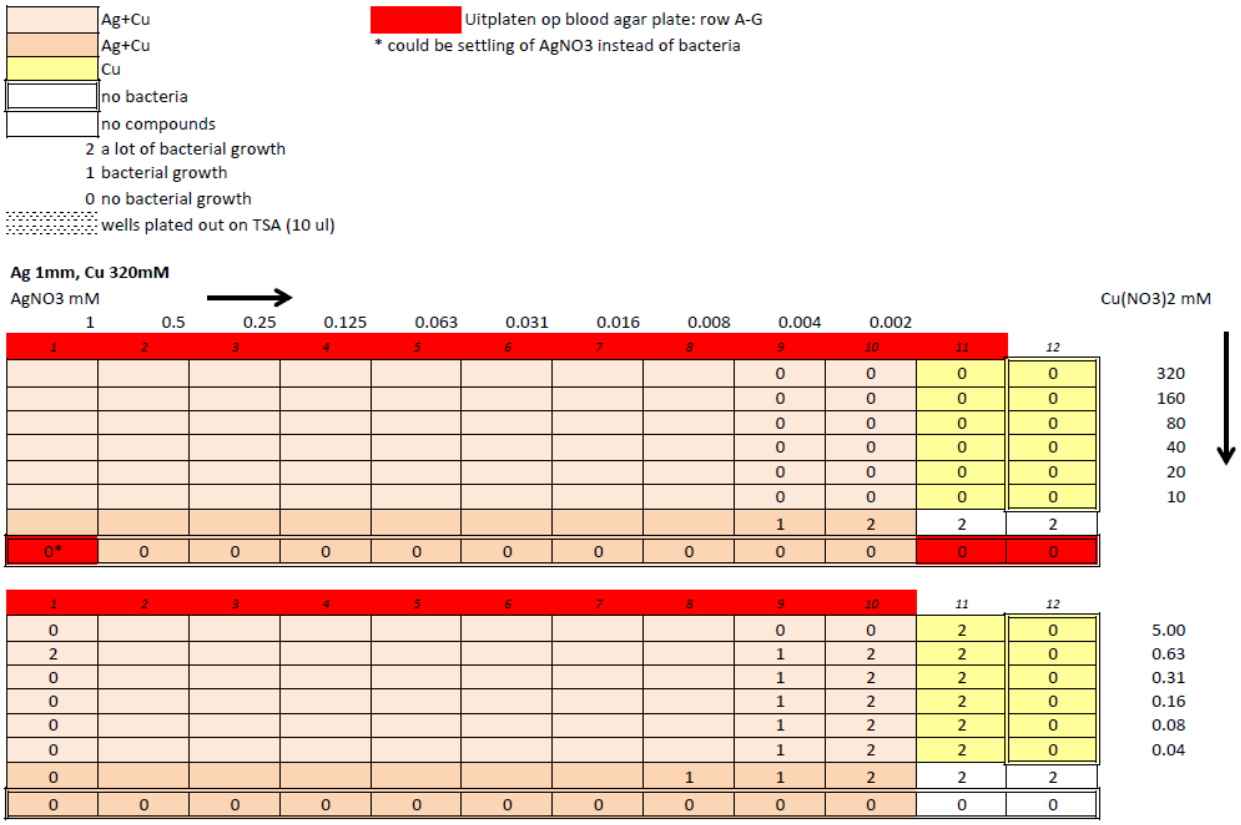

Figure 19: The checkerboard results. The cells without a number or with 0 indicated no growth, 1 indicated some growth and 2 a lot of bacterial growth. The white cells the positive control groups, with no antibacterial agents. The obtained MIC for Ag^{+} was 0.016mM, for Cu^{2+} was 10mM and the combined MIC 0.002mM Ag^{+} and 5mM Cu^{2+}.

F. CFU counts

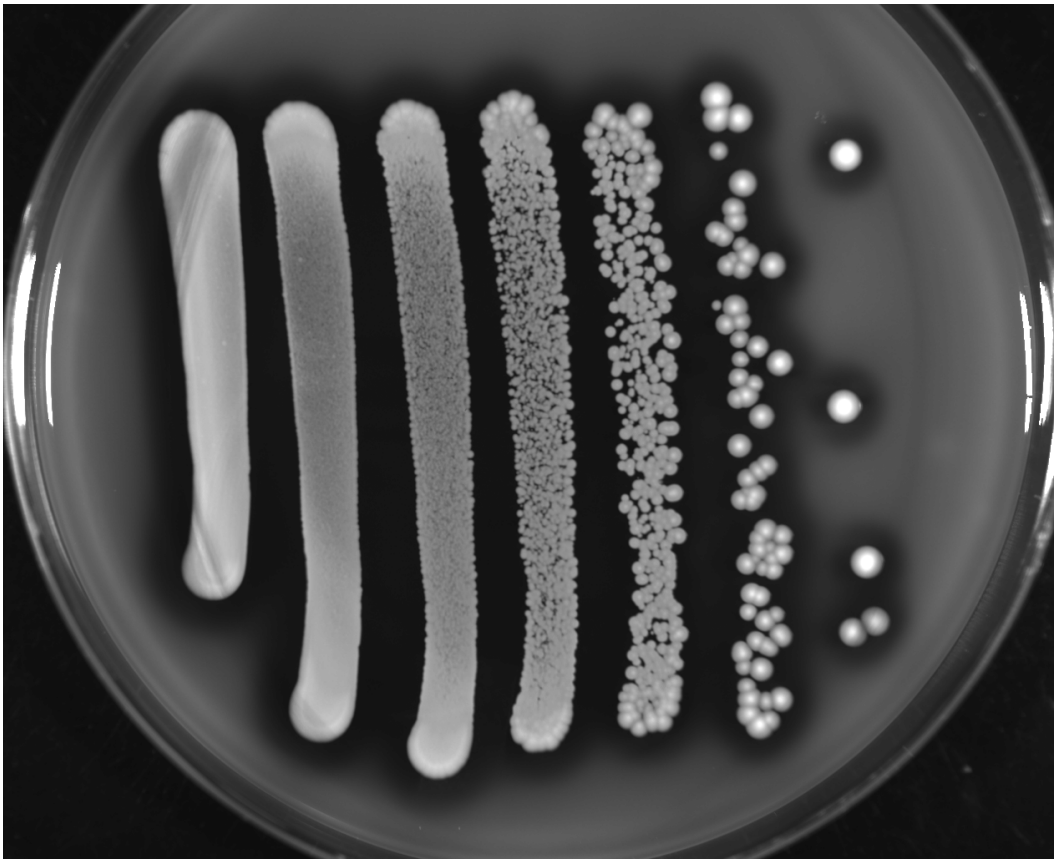

Figure 20: Blood agar plate with CFU count. Image of the blood agar plate with the positive control for the biofilm prevention test. Smear tests with dilution steps of 10 fold for each row from left to right. The CFU''s were defined by the white circles. The CFU count was defined by the column with the largest amount of CFUs capable of distinguishing between the different CFU's